

Magmatic and tectonic evolution of the Chaval Granite at the end of the Neoproterozoic, northwestern border of the Borborema Province

Arthur Jeronimo Santana Aragão^{1*} , Paulo Sergio de Sousa Gorayeb¹ , Marco Antonio Galarza¹ 

Abstract

The northwestern region of Borborema Province is represented by the Ceara Central and Northwest Ceara crustal blocks connected by an extensive transcurrent shear zone that represents the northern portion of the Transbrasiliano Lineament in a complex geological context, which brings together geological units of nature, origin, and ages of the Archean to the Paleozoic. In this scenario, there is a large amount of granitic bodies, with different natures, age and tectonic environment, but predominantly representing a more intense granitogenesis in the Paleozoic Neoproterozoic and early Paleozoic, with plutons emplaced in different stages of the Brazilian Orogeny. In this context, the Chaval Granite corresponds to an isolated body in the extreme northwest of Borborema Province, located near the Atlantic coast, in the northern states of Ceará and Piauí. It is an intrusive batholith housed in Siderian orthogneisses (Granja Complex) and in Neoproterozoic supracrustal rocks (Martinopole Group), but is partly covered by sedimentary rocks from the Parnaíba Paleozoic Basin (Serra Grande Group), and coastal Cenozoic deposits. Field data and petrographic studies highlight the porphyritic texture with microcline megacrystals involved in coarse matrix as a remarkable feature. The predominant petrographic types are granodiorites, with variations for monzogranites and tonalites. The predominant primary mineral constituents are perthitic microcline, oligoclase, and quartz; biotite and rarely hornblende as qualified minerals and additionally titanite, apatite, zircon, alanite, and opaque minerals. Another peculiar characteristic is the deformational features related to the installation of the Santa Rosa Transcurrent Shear Zone along its eastern flank. The effects of the transcurrent shear deformation led to the modification of the original magmatic fabrics in much of the eastern half of the batholith, generating various types of mylonites. Thus, the typically igneous textures preserved in the western half of the pluton were gradually replaced by tectonic fabrics, which initially evolved into proto-mylonites in the central portion of the body, grading to mylonites eastward, highlighting strongly stretching, comminution associated with dynamic recrystallization, highlighting the formation of microcline and plagioclase porphyroclasts in a mylonitic matrix, which are involved by mylonitic foliation. Geochemical studies reveal compositional similarities, compatible with petrographic classifications, in which they mostly present granodioritic composition, followed by monzogranites and tonalites, classified as I-type granites, peraluminous with compatible with the calcium-alkaline series. The geochemical signatures of the Chaval Granite indicate the character of the tectonic magmatic arc environment. U-Pb zircon analysis by Mass Spectrometry (LA-ICP-MS) indicates crystallization age of 633 Ma, placing it in the Neoproterozoic, late Cryogenic-Early Ediacaran period, being one of the oldest granitoids in northwestern Borborema Province, correlated to the granites of the Santa Quitéria Magmatic Arc in the Ceara Central Domain. Hf-T_{DM} model ages (2.65 to 2.13 Ga) and εHf(t = 633 Ma) values from -9.6 to -18.1 suggest incorporation of neoarchean and paleoproterozoic crustal sources in their formation with a long crustal residence time. Similar Sm-Nd data in whole-rock indicate Nd-T_{DM} model ages of 1.27, 1.72 and 2.04 Ga and negative εNd(t = 633 Ma) values of -2.64 to -9.13, indicating paleoproterozoic and mesoproterozoic sources, with considerable crustal residence time implying a more evolved nature.

KEYWORDS: Chaval Granite; Mylonites; Geochronology; Neoproterozoic; Santa Quitéria Magmatic Arc; Borborema Province.

INTRODUCTION

The Chaval Granite, the main object of the present study, outcrops near the Atlantic coast, north of Piauí and Ceará States, having as reference Chaval, Parnaíba, and Bom Princípio cities. It is a batholith of approximately 2,000 km², inserted in the Northwestern Ceará Belt (NWCEB) (Abreu *et al.* 1988), in the Northwestern Ceará Domain, on the northwest border of Borborema Province (Figs. 1 and 2).

The northwestern portion of the Borborema Province (BP), presents a wide variety of rocks from Archean to Paleozoic, with an emphasis on granite magmatism, highlighting bodies of varying sizes, natures, and ages, which are temporal markers of regional geological processes (Figs. 1 and 2).

The literature presents several studies related to granitoids in this region (Sial 1989, Brito Neves *et al.* 2000, Fetter *et al.* 2000, 2003, Bizzi *et al.* 2003, Arthaud 2007, Ganade de Araujo *et al.* 2013, 2014). However, although cartographically well-identified, the knowledge of these granite bodies still lacks fundamental data for their comprehension and contextualization in the tectonic evolution of northwestern BP, such as structure and relationships with the surrounding rocks, petrography, geochemistry, typological characterization and isotopic and geochronology with more robust methods, which

¹Universidade Federal do Pará – Belém (PA), Brazil.

E-mails: gorayebp@ufpa.br, arthurjsaragao10@gmail.com, antogt@ufpa.br

*Corresponding author.



are fundamental to discuss correlations with better known of the granitogenesis events in the region.

The granitogenesis in BP was divided into three main tectono-magmatic events recorded by Bizzi *et al.* (2003), approaching them as a succession of tectono-magmatic events related to the Brasiliano cycle, defined as follows: Supersuite I (early to syn-Brasiliano); Supersuite II (late-Brasiliano); and Supersuite III (post-Brasiliano).

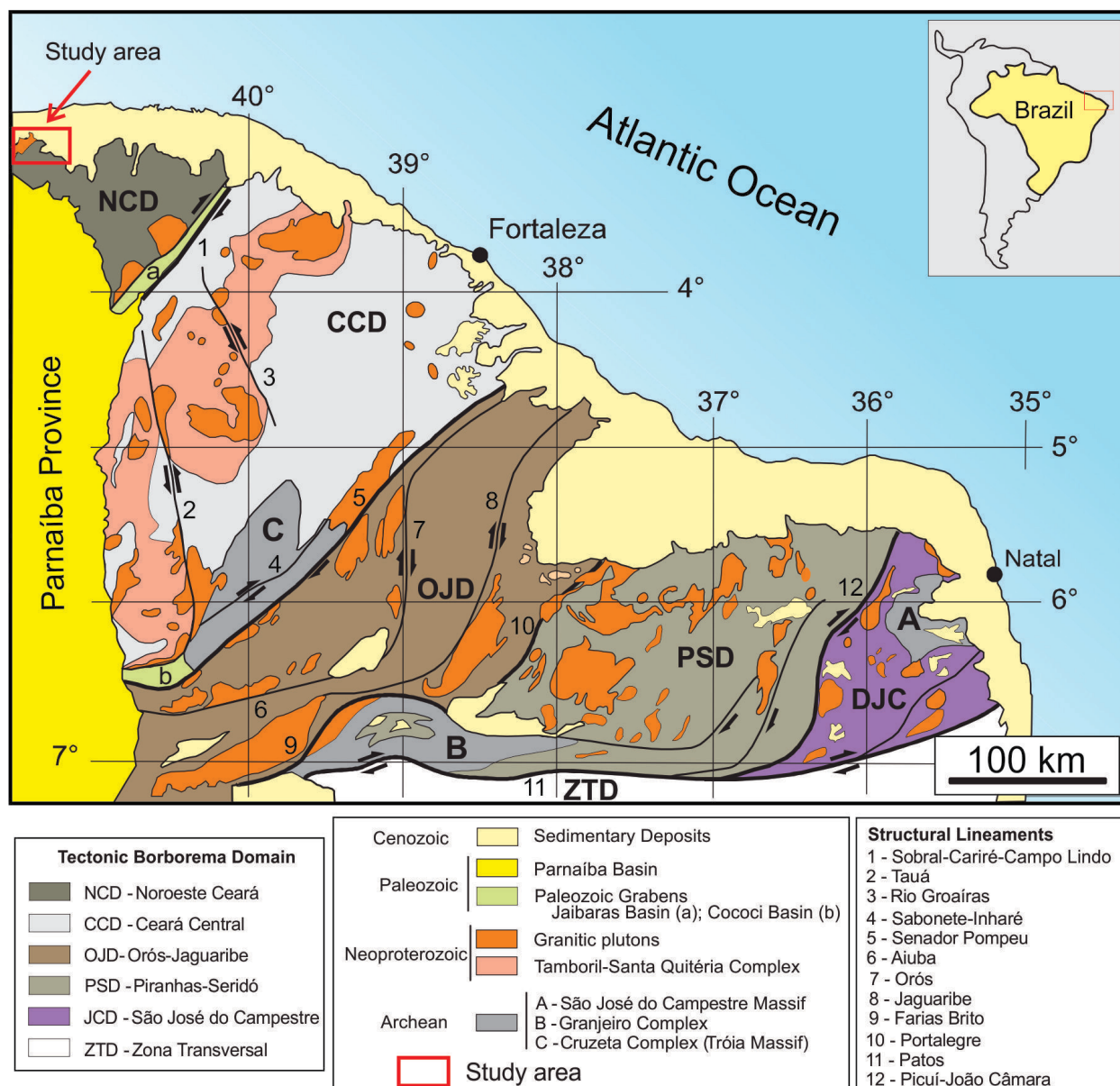
In the case of Chaval Granite, considering the absence of detailed petrographic studies, geochemical and isotopic data, and previous discrepant geochronological data, makes it difficult to correlate it with other known granites.

The study developed here shows new field data, detailed petrographic analyses, isotopic and geochemical data, new geochronological analysis approach of this important magmatic unit, complementing the gaps of previous works and clarifying a wide range of questions from the magmatic and tectonic nature, and the process of emplacement and structuring of the Chaval Granite. With these new data, we favor studies of correlation with other events in the region, discussions and interpretations about the meaning of this body in the NW evolutionary context of BP.

GEOLOGICAL CONTEXT OF THE NORTHWESTERN BORBOREMA PROVINCE

The BP is a large and important crustal compartment in the Northeast region of Brazil, with correspondence in the northwestern portion of the African continent, especially the orogenic systems of the Brasiliano-Pan-African cycle (Brito Neves *et al.* 2001). It represents a complex polycyclic evolution, recording ages from the Archean to the Neoproterozoic, with a marked influence of the Brasiliano/Pan-African cycle, which was responsible for the end of the amalgamation of the Gondwana Continent, between 660 and 570 Ma (Brito Neves *et al.* 2000).

The north-northwest portion of Borborema Province is divided into six major structural domains called Northwestern Ceará (NWCED), Central Ceará (CECD), Orós-Jaguaribe, Rio Piranhas-Seridó, São José do Campestre and Zona Transversal (Brito Neves *et al.* 2000, 2001, Arthaud 2007, Gomes *et al.* 2019) (Fig. 1). These domains are delimited by mega-transcurrent shear zones evolved at the end of the Neoproterozoic. A notable feature of this region is the large number of granitoid



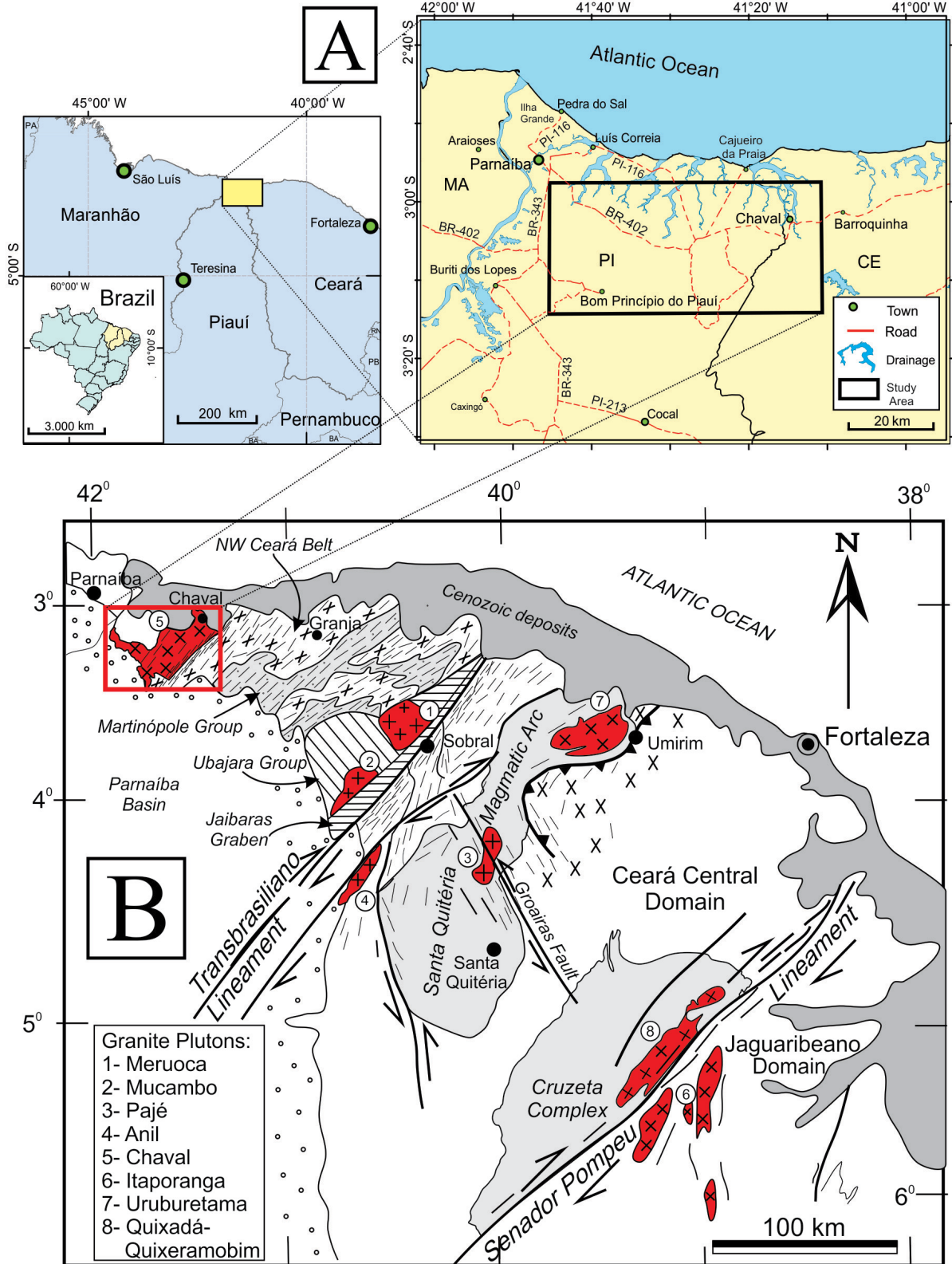
Source: adapted of Gomes *et al.* (2019).

Figure 1. Subdivision of the main tectonic domains of the northern portion of Borborema Province.

bodies, more precisely in the NWCED and CECD of nature, age and tectonic environments, which are important markers of tectonic events and magmatic evolution.

The study area is located in the NWCED, which is delimited by the Sobral-Pedro II Lineament that is part of the

Transbrasiliano Lineament to the north (Fig. 2). The NWCED consists of Paleoproterozoic basement (Siderian period), dated 2.35 Ga (Fetter *et al.* 2003), represented by the Granja Complex, constituted by tonalitic and granodioritic orthogneisses, amphibolites, sillimanite-garnet gneiss, migmatites, and granulites.



Source: adapted of Gorayeb and Lima (2014).

Figure 2. (A) Maps of the study area within the coastal region of the state of Piauí and extreme northwest of Ceará state; (B) Schematic geological map of the Northwest of Borborema Province highlighting the main and most representative granitoids of the region.

Neoproterozoic metasedimentary sequences constituted by psamite-pelitic-carbonate composition and metavolcanic rocks are represented by the Martinópolis Group (sillimanite quartzites, garnet-staurolite micaschists, amphibolites, calci-silicate gneisses, meta-rhyolites) and Ubajara Group (meta-conglomerate, meta-sandstone, meta-limestone, meta-arkose and pelitic slate). The Cambrian-Ordovician volcano-sedimentary successions constitute the Jaibaras Group (conglomerate, sandstone, arkose, siltstone and pelites) and Parapui Suite (intermediate and alkaline basalts, rhyolite, volcanoclastic and pyroclastic rocks), (Nascimento & Gorayeb 2004), which are sectioned by post-orogenic granite plutons (Meruoca Suite) (Gorayeb *et al.* 1988, Abreu *et al.* 1988, Nascimento & Gorayeb 2004, Archanjo *et al.* 2009, Gorayeb & Lima 2014). To the southwestern of Chaval city, there is the Brejinho Nepheline Syenite, a small peralkaline pluton, dated at 554 ± 11 Ma, intrusive in orthogneisses of Granja Complex which also intersects the Santa Rosa Shear Zone, related to the extensional tectonic environment of the Neoproterozoic-Paleozoic boundary (Gorayeb *et al.* 2011).

GRANITOGENESIS OF THE NORTHWESTERN BORBOREMA PROVINCE

The Neoproterozoic in the northern Borborema Province is marked by the building of orogens related to the Brasiliano Cycle with intense magmatic activity, diversified granitogenesis, development of extensive shear zones, and formation of metamorphic supracrustal successions that have reached metamorphic conditions of high-amphibolite to granulite facies (Brito Neves *et al.* 2000, Almeida *et al.* 2002, Cavalcante *et al.* 2003, Arthaud 2007, Ganade de Araujo *et al.* 2014, Amaral *et al.* 2015).

The granitoids were grouped according to chronological intervals of emplacement from 644 to 520 Ma, as follows:

- Normal calcium-alkaline;
- high potassium calcium-alkaline, with shoshonitic affinity;
- syenogranite, quartz syenite and syenite with shoshonitic affinity;
- biotite granite, transitional between alkaline and shoshonitic; and
- biotite syenogranite co-magmatic with basalt and dacite (younger ages) (Sial 1989, Ferreira *et al.* 1998, Guimarães *et al.* 1998).

Bizzi *et al.* (2003) proposed compartmentalizing the granitogenesis of the Borborema Province in a succession of magmatic pulses called Supersuite I (Early to Syn-Brasiliano), Supersuite II (Tardi-Brasiliano), and Supersuite III (Post-Brasiliano). The Syn and Tardi-Brasiliano (Supersuite I) have as representative the Santa Quitéria batholith as part of Tamboril-Santa Quitéria Complex. The Supersuite III is represented by the Meruoca Suite (granites Meruoca, Mocambo, Serra da Barriga, Pajé, Anil plutons, and Aroeiras dyke swarm) and Brejinho Nepheline Syenite pluton, whose bodies are intrusive either in metasedimentary rocks of the Ubajara and Jaibaras groups, or in gneisses and supracrustal rocks from the Ceará and Granja Complex (Gorayeb *et al.* 1988, Gorayeb & Lima 2014).

At the northwestern edge of the Borborema Province, other granitoids in isolated plutons present deformational effects such as the Pedra do Sal, Chaval, and Tucunduba granites, which are cut by transcurrent shear zones (Gama Jr. *et al.* 1988, Gorayeb & Lima 2014) and are certainly correlated to older events as discussed above.

Granitoids of the Tamboril-Santa Quitéria Complex (Magmatic Arc)

The Tamboril-Santa Quitéria Complex (TSQC) include a group of the granitoids from northwestern of BP, which are the oldest granitic rocks of the Neoproterozoic rocks of CECD and are distributed over approximately 40,000 km² with NE-SW structural trends (Fig. 2). It is a granitic-gnaissic-migmatite complex whose main characteristic is the intense migmatization associated with a large volume of anatectic granites.

Fetter *et al.* (2003) reported age of 665 ± 5 Ma (U-Pb in zircon) for the volcanic rocks flanking the batholith in the TSQC. The more deformed granitic plutons revealed ages dated between 637 ± 6 and 624 ± 1 Ma, with possible magmatism continuation until 591 Ma. These authors also stated that this magmatism is related to plutonism in a continental magmatic arc (Santa Quitéria Magmatic Arc) whose intense deformation and anatexis resulting from the Brasiliano/Pan-African collision hinders the reconstruction of the arc geometry. In addition, it is suggested that the granitic plutonism represents the last stages of the arc evolution, with a progressive increase of the crustal participation, especially by remelting of the earlier magmatic material.

Still, Fetter *et al.* (2003) divided the granitoids into four main groups, which represent the evolution phases of the magmatic arc, described below:

- Group 1: comprises pre-collisional granitoids, consisting of diorites to granodiorites, with high Mg and low K that represent the most primitive phase of the arc's continental magmatism. Gray granodiorites, sometimes deformed and metamorphosed, that were partially removed in the later stages of arc development predominate. They are associated and mixed with schists, gneisses with different migmatization degrees. Mafic types with irregular distribution and dimensions, such as amphibolites, are also observed. In contrast, there are heterogeneous, more felsic migmatite complexes that host extensive mafic bodies regionally, but also occur around newer plutons with megacrystals;
- Group 2: includes more evolved pink and gray granites associated with nebulite migmatites, represented by quartz-rich rocks, from granodiorite to granite composition. They represent higher degrees of pre-collisional diorite removal;
- Group 3: it is represented by porphyritic granodiorites and monzogranites, with feldspar megacrysts, weakly deformed. Locally, these rocks contain varying amounts of rounded or irregular diorite enclaves, with no major signs of magma interaction, representing phases of non-plutonic dikes. This association is interpreted as representing the emplacement of the granites related to the regional phase of tension during arc development. This group is significantly less abundant than the other igneous associations of the TSQC;

- Group 4: represents the final phase of the magmatic arc development that is characterized by the emplacement of granitoids with high K and low Ca, predominantly monzogranitic composition with feldspar megacrysts. They include calcium-alkali and alkali-calcium plutons. This group represents the progressive gradual participation of the crustal materials, mainly with remelting of the first two groups, suggesting the existence of several magmatic pulses in the final stages of arc development.

These first two lithological groups are characteristic of the early arc magmatism in terms of composition, structure, and evolution.

Ganade de Araujo *et al.* (2014) also provided data supporting the idea that the granitoids of the TSQC represent different phases of a magmatic arc, dividing it into three main phases, as follows:

- Juvenile arc magmatism (880 to 800 Ma): this phase is basically represented by granodiorites and tonalities of the Tamboril and Lagoa Caiçara units, and originates in an early subduction zone in extensional environment with great contribution of juvenile magma attributed to the consumption of the Goiás-Pharusian Ocean. This phase still accounts for the continuation of the subduction, development of extensional basins of retro-arc with magmatism associated and supracrustals derived from both the arc and the continent (crustal);
- Magmatism related to mature arc of the Andean type (660 to 630 Ma): it represents younger granitoids of the Santa Quitéria and Boi units, and a set of gneisses and granitoids from the Lagoa Caiçara unit. At this stage, the magmatism sources are both mantelic and crustal, with characteristics of a more mature stage related to subduction environment;
- Reworking of arc rocks in the event of crustal anatexis (620 to 610 Ma): this phase is basically represented by granitic neosome, grouped in the Tamboril unit, resulting from the refusion of the surrounding protolith, mainly intermediate composition orthogneisses of the Lagoa Caiçara and Santa Quitéria units and small portions of metasedimentary rocks of the Ceará Complex. The isotopic composition of neosome reflects an early source of crustal components. This phase represents the end of the collision with two subductions of the continental crust to the west and east of the Santa Quitéria Magmatic Arc (back-arc basin).

Post-orogenic granitoids

A wide range of granite plutons is distributed along and near the main axis of the Sobral-Pedro II Lineament (TBL). They represent post-orogenic bodies intrusive in the volcano-sedimentary successions of the Ubajara and Jaibaras groups, as well as in the basement gneisses. They are bodies housed in shallow depth, at higher crustal level, developing an expressive aureole of thermal metamorphism in larger bodies, that reached maximum conditions in pyroxene-hornfels facies (Danni 1972, Gorayeb *et al.* 1988, Gorayeb & Coimbra 1995). This magmatism is related to the extensional tectonic event that generated horst and grabens, such as Jaibaras

Graben, in the interface between the CECD and NWCD of the Neoproterozoic-Paleozoic boundary. They were grouped in the Meruoca Granitic Suite constituted by the Meruoca, Mucambo, Serra da Barriga, Anil and Pajé granitic plutons, and the Aroeiras dike swarm and other smaller bodies (Costa *et al.* 1979, Gorayeb *et al.* 1988, Gorayeb & Abreu 1991, Gorayeb *et al.* 1993, Gorayeb & Soares 1994, Nascimento 2012, Gorayeb *et al.* 2014a, 2014b). To the southwest of the city of Chaval, a peralkaline pluton (Brejinho Nepheline Syenite) is also correlated to this extensional tectonics (Gorayeb *et al.* 2011).

GEOLOGY OF THE AREA

The Chaval Granite is located at the northwestern edge of the Borborema Province, in the Northwest Ceará Belt (Abreu *et al.* 1988, Gorayeb & Lima 2014). The principal geological units in the region comprise Paleoproterozoic orthogneisses (Granja Complex), Neoproterozoic supracrustal rocks (Martinópolis Group), Paleozoic sedimentary rocks of the Parnaíba Basin and recent coastal sedimentary cover (Figs. 3 and 4).

The Granja Complex, the oldest unit in the region, has been dated by Fetter *et al.* (2000) at 2.35 Ga (Siderian) and consists of extensive areas of tonalitic and granodioritic orthogneisses, partially migmatized (Fig. 4A), paragneisses bands with sillimanite, garnet, biotite and mafic granulite, enderbite with charnockite neosomes, together with quartzites, banded ferrous rocks and amphibolites.

The Martinópolis Group consists of supracrustal Neoproterozoic sequences that include varied mica-schists with muscovite, biotite, garnet, staurolite, kyanite and/or sillimanite (Fig. 4B); quartzite with muscovite and/or sillimanite, aluminous paragneisses, calc-silicate rocks, marbles, amphibolites, ferruginous, manganese or graphite schists, and felsic metavolcanics (Abreu *et al.* 1989, Santos & Hackspacher 1992, Santos *et al.* 2008). The U-Pb dating in metariorite zircon showed an age of 777 ± 11 Ma (Fetter *et al.* 2003).

The Chaval Granite stands out as an expressive body of batholithic dimensions in the northwest end of the area, bordered by the Santa Rosa Transcurrent Shear Zone (SRTSZ) to the east, disappearing under sedimentary deposits to the south and west (Figs. 3 and 4C).

An alkaline pluton named Brejinho Nepheline Syenite (Gorayeb *et al.* 2011) is a small alkaline body located southwest of the studied area, showing intrusive relationships in orthogneisses of the Granja Complex and sectioning the SRTSZ. Rb-Sr dates in whole-rock indicate age of 554 ± 11 Ma (Gorayeb *et al.* 2011). This small pluton is considered an important representative of post-tectonic magmatic phases related to the extensional tectonics of the early Paleozoic, which formed the Jaibaras grabens system (Gorayeb *et al.* 1993).

In addition, the Meruoca Granitic Suite (Gorayeb *et al.* 2014a, 2014b) represents the magmatic phase of the beginning of the Paleozoic, with the following ages: Meruoca Granite — 523 ± 9 Ma (Archanjo *et al.* 2009); Mucambo Granite — 542 ± 6 Ma, U-Pb zircon (Fetter 1999); Aroeiras dikes associated with the Meruoca Granite — 523 ± 20 Ma (Teixeira *et al.* 2010), Serra da Barriga — 522 ± 7 Ma (Mattos *et al.* 2007),

Anil Granodiorite — 587 ± 5 Ma (Gorayeb & Lafon 1995),
Pajé Granite — 530 ± 3 Ma (Gorayeb *et al.* 2013).

In the southwestern part of the area, Paleozoic sedimentary rocks of the Serra Grande Group, consisting of thick sub-horizontal layers of conglomerate and sandstones representing the basal unit of the Parnaíba Basin, are placed on non-conformities in the units described above (Fig. 4D).

FIELD ASPECTS AND PETROGRAPHY OF CHAVAL GRANITE

Initially named “Chaval-type granitoid” in the Jaibaras Project (CPRM) by Costa *et al.* (1979), the Chaval Granite defines a batholith of approximately 2,000 km² that outcrops near the Atlantic coast between the states of Piauí and Ceará, having as reference the cities of Bom Princípio, Parnaíba (PI) and Chaval (CE). Although a large part of the body is covered by sedimentary rocks from the Parnaíba Basin, to the southeast, and by Cenozoic sediments from different coastal environments, such as wind, alluvial, and mangrove deposits, large rock exposures of Chaval Granite occur along the drainages and in hills and boulders with bulging tops, without major relief highlights. On the eastern side of the study area, the granitoid presents an intrusive relationship with the orthogneisses of the Granja Complex, which are difficult to recognize due to the deformation imposed by the SRTSZ, demarcating a tectonic contact.

The petrographic analysis of 36 samples representing the varied petrographic facies of the Chaval Granite was performed

using conventional optical microscopy, for mineralogical characterization and quantification, and textural/microstructural analysis. Modal mineralogical analysis of nine representative samples was performed using SWIFT Automatic Point Counter from the Petrology Laboratory of the Graduate Program of Geochemistry and Petrology/Geosciences Institute/Federal University of Pará (LAPETRO/PPGG/IG/UFPA), with 1,200 or 1,500 counts according to sample grain variation. The petrographic classification was based on Streckeisen (1976), Le Maitre (2002), Fettes and Desmons (2008), and Paschier & Trouw (1998), and the modal results were plotted as Q-A-P and Q(A + P)-M' diagrams.

The samples analyzed were widely distributed in the outcropping areas of the granitic body (Fig. 3). Despite its batholithic dimensions, it presents relatively homogeneous mineralogy but with significant textural/microstructural variation that changes from typically magmatic features to mylonitic structures, reflecting the SRTSZ movement at the eastern interface of the pluton with the gneiss and schists country rocks.

The Chaval Granite has two fabric domains with very distinct characteristics, mainly from the structural point of view. The first domain comprises typically plutonic rocks with preserved magmatic features, represented by porphyritic granites occupying the central and western portions of the body (Figs. 5 and 6). The second domain consists of mylonitic granites with striking records of shear deformation and gradually varying intensity, distributed since central until eastern portions of the body, and resulted from the establishment of SRTSZ (Figs. 3 and 6).

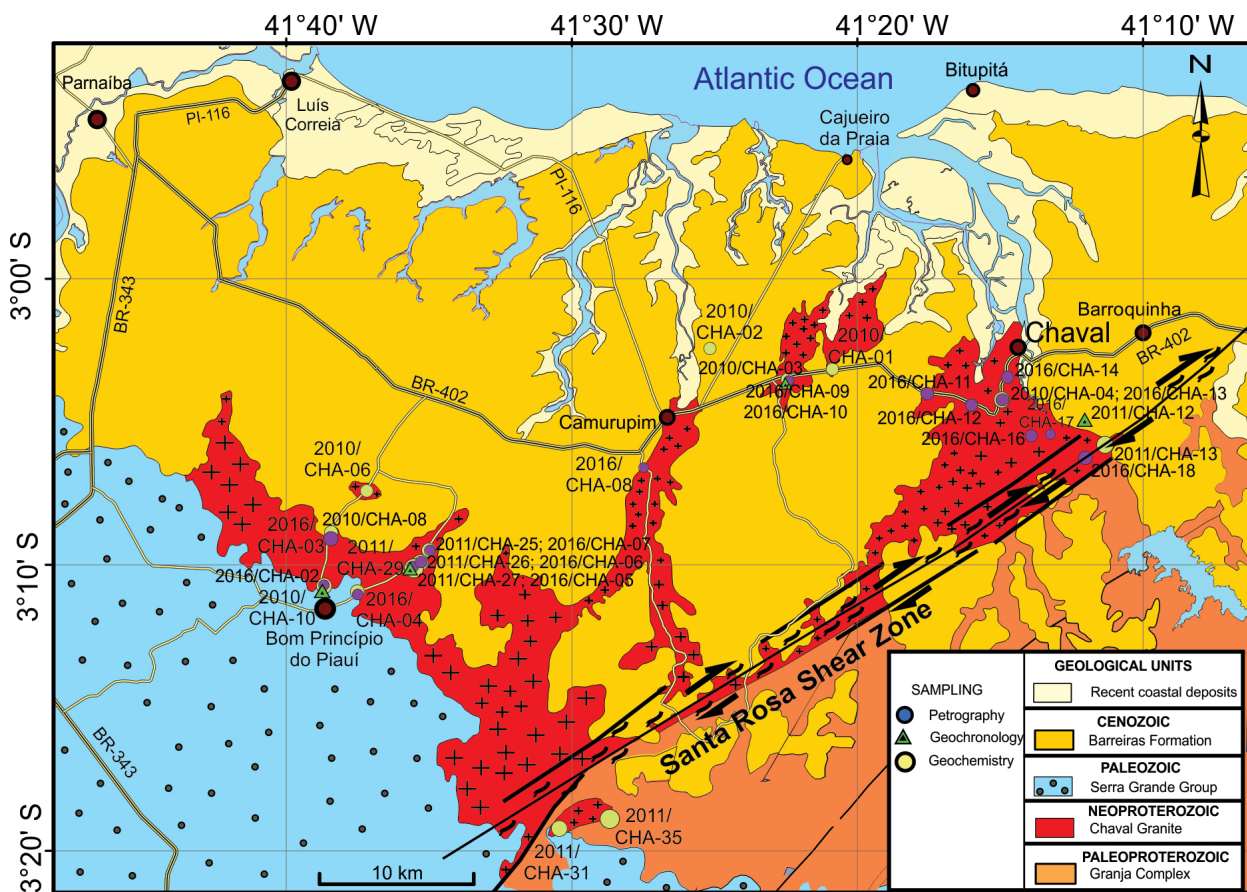


Figure 3. Geological map of the Chaval-Parnaíba region composed of the main geological units with the sampling point used in this work. Prepared from CPRM data and mapping in this paper.

Lenticular and irregular enclaves or schlieren sheets (concentration of biotite) are oriented according to the magmatic flow (Figs. 5D and 5F). Some with irregular shapes, fine granulation, and intermediate composition with xenocrysts are also observed (Figs. 5D and 5E). Its origin can be related to magma mixing. Schlieren types concentrated in biotite can be explained as residues from the fusion of the original sources of the magma (restites).

Small intrusive bodies, hololeucocratic pegmatitic and aplitic veins and dikes, rich in alkali-feldspar and quartz, are observed sectioning the main rocks. They sometimes present small laccoliths or inverted funnel-shape, which represent the most evolved phases of the evolutionary magmatic process of the Chaval Granite (Fig. 5C).

The plutonic-type textures are located in the central portion to the west of the body. On the opposite side, from the central portion to the east, the records are typical of shear deformation with progressive transformations, with greater deformation intensity toward the SRTSZ. The main petrographic types within the domains will be described below.

Porphyritic granites

Low to non-deformed domain of the granite occurs in the western portion of the batholith close to the cities of Buruti dos Lopes, Parnaíba, and Bom Princípio, where magmatic

characteristics are preserved with little or no record of ductile deformation. They are porphyritic granites, composed of megacrysts of alkali-feldspar (up to 10 cm), with remarkable oscillatory zoning, in coarse grain size phaneritic matrix. The granites are leucocratic, equigranular (in their matrix), with mineral association consisting of microcline, plagioclase, quartz and titanite in varying amounts, followed by biotite, as well as allanite, zircon, apatite, and opaque minerals as accessory phases.

The most striking structures are magmatic flow layering, defined by the preferential alignment of tabular microcline phenocrysts (Fig. 5A).

The accumulation of microcline megacrysts in concentration between 60 and 90% in relation to the matrix is common (cumulus microcline megacrysts with intercumulus), characterizing cumulate syenitic or quartz syenitic rocks (Fig. 5B). This is related to the magmatic differentiation process in an important phase of granitic pluton evolution (Gill 2010).

Small leucogranite diapiric laccolith, inverted funnel-shaped and dike-like bodies, controlled by distensional fractures, developed late in the magmatic evolution (Fig. 5C).

The modal analysis data of undeformed granite samples (Tab. 1) reveal only small variation in the mineralogical content, so that in the Streckeisen diagram (Le Maitre 2002) the samples plot predominantly in monzogranite and granodiorite fields, except for a sample that plots in the tonalite field

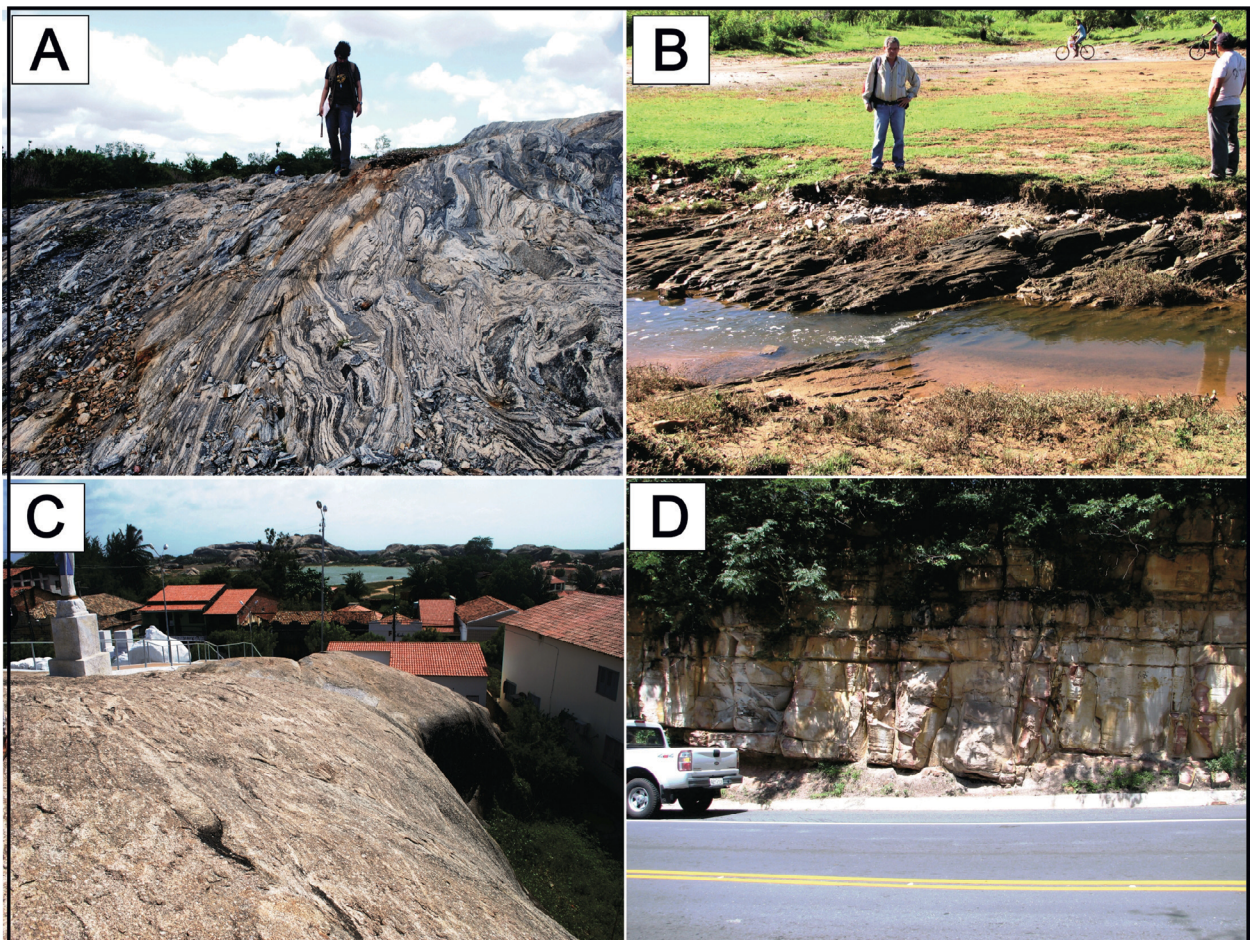


Figure 4. General aspects of the geological units of the Chaval region: (A) Large exposure of orthogneisses migmatized and folded with amphibolite enclaves of the Granja Complex; (B) Garnet-biotite schist from the Martinopole Group on the eastern flank of the Chaval Granite; (C) Extensive outcrop of the Chaval Granite exposed in the form of a large bulging mass in the center of the Chaval city; (D) Stratified sandstones of the Serra Grande Group exposed in a section on BR-343.

(Fig. 7). In this diagram, the samples show a slight alignment comparable to the calcium-alkaline trend of granite series of Lameyre and Bowden (1982).

Microscopic observation shows that tabular euhedral phenocrysts are mainly perthitic microcline (rarely plagioclase), displaying Carlsbad twinning, usually zoned concentrically whose crystal growth zones are demarcated by the inclusion of biotite lamellae in aligned trails. The megacrystals are supported by a coarse-grained matrix with a hypidiomorphic granular texture, consisting predominantly of well-developed crystals of plagioclase, microcline, quartz, and biotite (Fig. 8).

Deformed granites

The fabric observed in the deformed granite is related to the SRTSZ activity. While maintaining the porphyroid aspect, with deformational fabric show gradually increasing inf deformation from west to east, in the eastern portion of the batholith, overlapping the original igneous fabric. This domain corresponds to what Gorayeb and Lima (2014) defined in their structural map as Domain B (subdomains B1 and B2), with representative outcrops in the city of Chaval and surrounding areas (Fig. 3). Figure 9A shows an extensive outcrop where deformed granitoids occur.

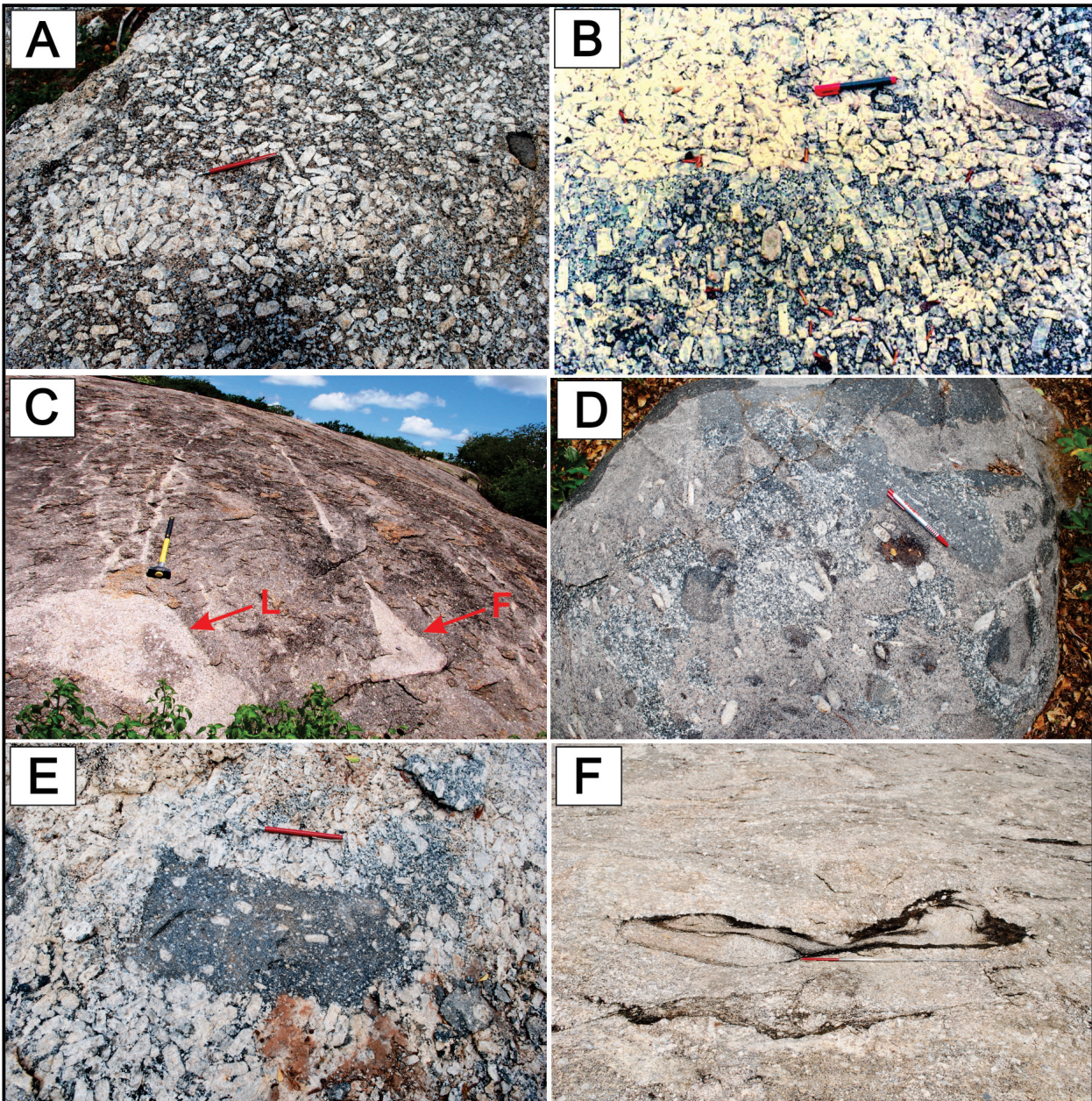


Figure 5. Features found in the Magmatic Domain of Chaval Granite: (A) Porphyritic texture with microcline megacrystals oriented according to the magmatic flow (magmatic layering). Note local accumulation of microcline megacrystals preferably aligned, denoting magmatic flow in channels and conduits within the residual magma; (B) Porphyritic granite with magmatic flow structure with subvertically aligned microcline tabular megacrystals in the lower half of the photo; and in the upper portion, accumulation of these crystals generating sienitic cumulates (magmatic differentiation) by gravitational rise in the residual liquid; (C) Small intrusive leucogranites bodies in the form of inverted funnel-shape (F) and laccolith (L) with flow upward in small conduits, representing late phase of the magmatic differentiation process (see red arrows); (D) Several mafic enclaves encased in porphyritic granite, forming hybride microdiorite with flow magmatic structure, denoting magma mixing process; (E) Small mafic-microdioritic enclaves with irregular contacts and shapes and xenocrysts, enclosed by granite with cumulated megacrystals aligned (magmatic layering) related to magma mixing; (F) Schlieren-type enclaves (biotite concentrates) oriented according to the magmatic flow.

Based on the deformational aspects, two subgroups were identified. The first subgroup (B1) is represented by partially deformed rocks, exhibiting evidence of deformation, but preserving the original magmatic (plutonic) features, characterizing the beginning of the mylonitic deformation, affecting especially quartz crystals of the matrix (Fig. 6). The microcline megacrysts are not significantly modified, maintaining the original shapes only with microfractures and crystal segmentation (Figs. 6A and 6C). On the other hand, the reduction of the matrix granulation (comminution) from coarse to medium- or fine-grained is already observed. This process developed a spaced foliation defined by the stretching and preferential orientation of quartz crystals and biotite lamellae, characterizing the ductile deformation (Figs. 9B–9F). With these limited modifications of

primary fabric, the rocks are classified as protomylonites based on the mylonite classifications of Bell and Etheridge (1973) and Sibson (1977).

In the B2 subgroup, the igneous textures appeared more modified, showing the higher intensity of the shear processes, with typical mylonitic features, as indicated by Passchier and Trouw (1998) and Trouw *et al.* (2010) (Fig. 10). They include strong foliation transposition and mineral stretching, tectonic banding, sub-grain, recrystallized polygonal grain aggregates, and mylonitic anastomosed foliation (Figs. 10A–10F). Microcline porphyroclasts (originally phenocrysts) are present as stretched almond shape, sometimes acquiring a sigmoidal shape (Figs. 10B–10D), immersed in the mylonite matrix represented by ribbon quartz crystals and strongly oriented

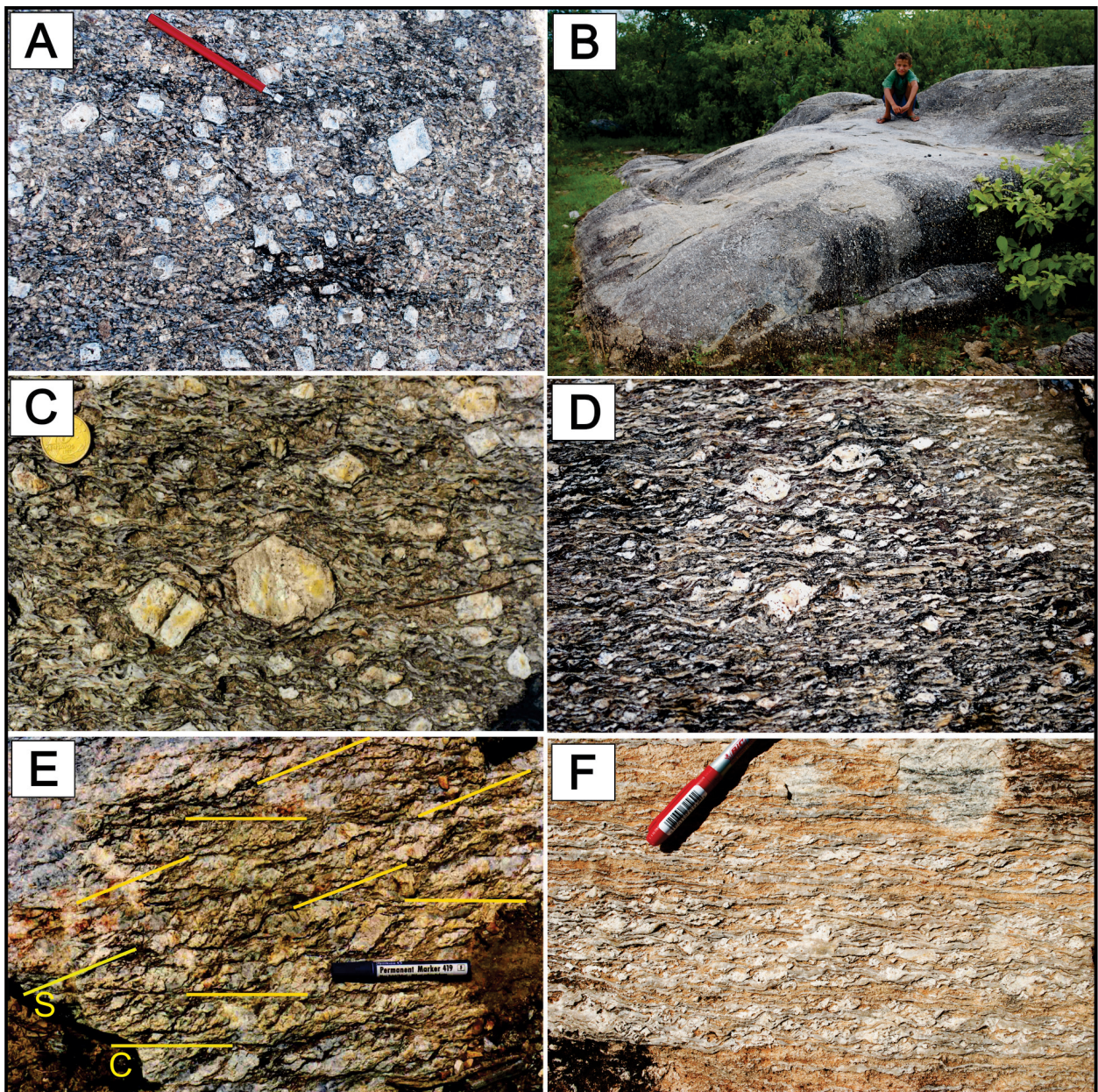


Figure 6. Main structural features found in the deformed domain: (A) Partially deformed granite (B1 subgroup) with centimetric euhedral phenocrysts immersed in a deformed matrix of medium granulation; (B) Chaval Granite extremely milonitized with subvertical foliation featuring ultramylonite domain; (C) Detail of partially preserved zoned euhedral microcline phenocrysts, and some porphyroclasts, encompassed by anastomosed milonitic foliation defined by ribbon quartz; (D) Sigma-shape porphyroclasts immersed in anastomosed milonitic matrix indicating dextral kinematics; (E) S-C foliation indicating dextral kinematics; (F) Extremely deformed milonitic granite with predominance of ribbon quartz structures, and sigmoidal feldspar porphyroclasts indicating dextral kinematics.

biotite lamellae and fine quartz-feldspathic aggregates (Figs. 6F, 10C, 10D and 10F). The occurrence of S-C fabric is common (Fig. 6E). In this case, the fine or medium-grained rocks are a product of intense comminution by dynamic recrystallization. Based on the classification proposal by Trouw *et al.* (2010) can be classified as medium-grade mylonites.

GEOCHEMISTRY

The analytical results of the geochemical studies performed on 13 samples are shown in Tables 2. The major, minor and trace elements analyses were determined by ICP-ES (Inductively Coupled Plasma-Emission Spectrometry), ICP-AES, ICP-MS, and AES performed in the ACME-Analytical Laboratories Ltd. in Vancouver, Canada. The samples were digested with

Table 1. Modal composition of the rocks of the preserved domain of the Chaval Granite.

		MONZOGRANITE				GRANODIORITE				TONALITE
		2016/ CHA-02	2016/ CHA-07	2016/ CHA-09	2016/ CHA-10	2016/ CHA-03	2016/ CHA-05	2016/ CHA-06	2016/ CHA-08	2016/ CHA-04
Quartz		24.8	29.8	27.9	29.8	29	27.3	28.2	25.3	26.8
Plagioclase		23.3	31.3	30.5	30.2	26.7	42.5	42.1	38.8	37.1
Microcline		23.2	30.2	25.1	21.2	13.4	20.1	22.4	12.9	2.8
Biotite		25.5	7.4	15.9	16.9	26.1	8.3	6.1	20.8	28.9
Titanite		1.7	0.4	0.3	0.4	2.8	0.6	0.6	1.6	3.7
Zircon		0.5	0.2	0.1	0.5	0.6	0.4	0.2	0.2	0.3
Apatite		0.5	0.3	0.1	0.5	0.7	0.4	0.2	0.2	0.2
Opaque minerals		0.5	0.4	0.1	0.5	0.7	0.4	0.2	0.2	0.2
Total		100	100	100	100	100	100	100	100	100
Felsic		70.7	91.8	83.7	82.2	70.4	90.7	93.1	77.4	67.2
Mafic (M)		30.3	8.7	16.5	18.8	30.9	10.1	7.3	23	33.3
Transformed to 100%	Q+A	34.86	32.64	33.41	36.70	41.97	30.37	30.42	32.86	40.18
	P	32.71	34.28	36.53	37.19	38.64	47.27	45.42	50.39	55.62
	M'	32.42	33.08	30.06	26.11	19.39	22.36	24.16	16.75	4.20
	Q	34.86	32.64	33.41	36.70	41.97	30.37	30.42	32.86	40.18
	A	32.42	33.08	30.06	26.11	19.39	22.36	24.16	16.75	4.20

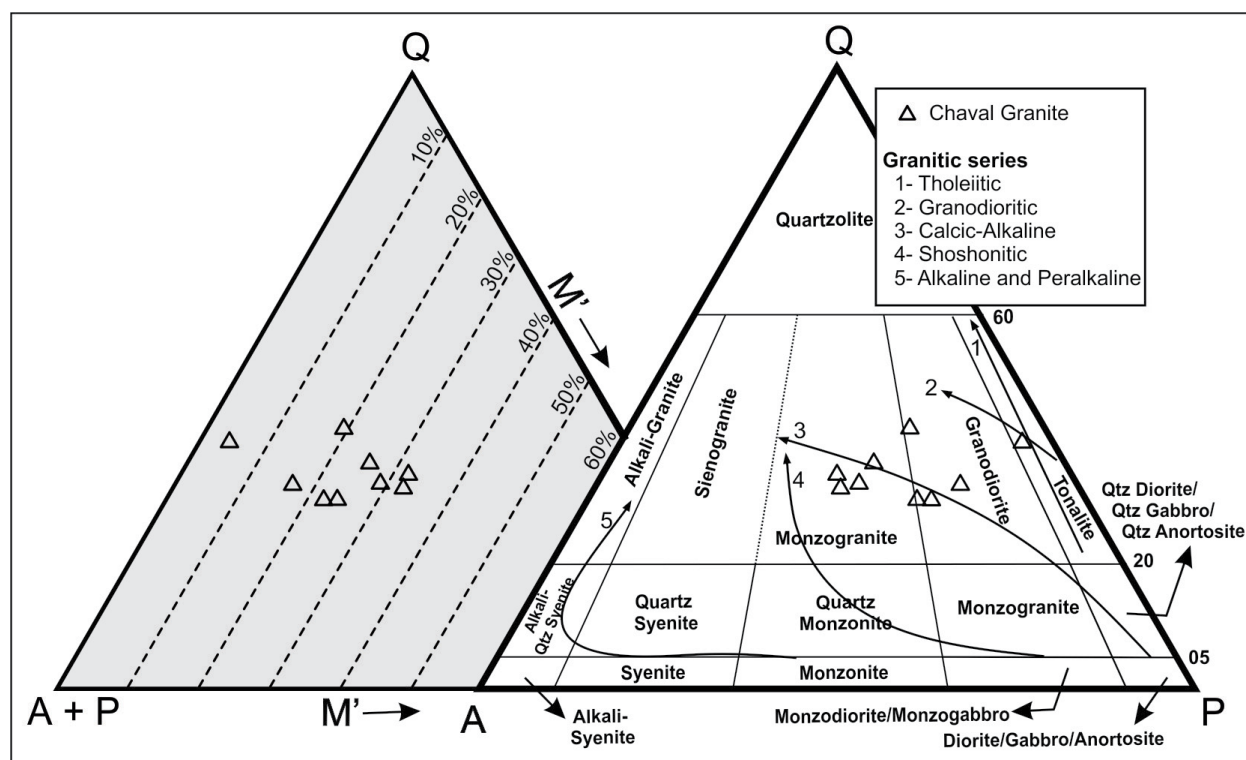


Figure 7. QAP and Q(A+P)M' diagrams from Streckeisen (1976) and Le Maitre *et al.* (2002) with the modal composition of the samples representing the magmatic domain and showing trends in the composition of the Lameyre and Bowden (1982) granite series.

lithium metaborate/tetraborate and the SiO_2 , TiO_2 , Al_2O_3 , $\text{Fe}_2\text{O}_3(\text{t})$, MgO , CaO , MnO , Na_2O , K_2O , and P_2O_5 contents were determined using the following detection limits: $\text{SiO}_2 = 0.02\%$; $\text{Al}_2\text{O}_3 = 0.03\%$; $\text{Fe}_2\text{O}_3 = 0.04\%$; K_2O ; CaO ; MgO ; Na_2O ; MnO ; TiO_2 , and $\text{P}_2\text{O}_5 = 0.01\%$.

The trace elements (Rb, Sr, Ba, Ga, Y, Zr, Nb, U, Th, Cr, Ni, V), including rare earth elements (La, Ce, Nd, Sm, Eu, Gd, Dy, Er, Yb, Lu), were also determined using the following detection limits: Cs, Sn, Cu, and Ni = 1 ppm; Ba, Ga, Hf, Nb, Rb, Sr, V, Zr, La, Ce, Eu, Gd, Dy, Ho, Er, Tm, Yb, Co, and Zn = 0.5 ppm; Nd = 0.4 ppm; Hg, Ta, Th, Ti, U, W, Y, Sm, Lu, Bi, Cd, and Sb = 0.1 ppm; Pr and Pb = 0.02 ppm. Further descriptions of ACME-Analytical preparation packages and analytical methods can be found on their webpage (<http://www.acmelab.com/>).

The loss on ignition (LOI) (mainly H_2O) was determined using thermogravimetric techniques, in which a predetermined sample amount is dried at 105°C to remove moisture, followed by burning at $1,000^\circ\text{C}$. The samples presented total values close to 100%, indicating low fire loss values and good analytical quality. To calculate the parameters and use in the geochemical diagrams, the concentrations of the major elements were recalculated using the conversion factor for volatile correction, according to the procedures by Rollinson (1993), Wilson (1989) and Gill (2010).

The discriminant diagrams of element variation and correlation with the obtained geochemical data were performed

using the GCDKit 3.0 software. The purpose was to define the nature of the magmatism and the tectonic environment of body emplacement, providing knowledge on the processes that influenced the Chaval Granite formation.

The data in Tables 2A and B show small differences in the contents of the major elements in the studied samples, reflecting the original composition of the petrographic types.

In general, the studied rocks present high SiO_2 (64 to 75%), Al_2O_3 (~14 to 16%), and alkalis (7 to 8.5%) with $\text{K}_2\text{O}/\text{Na}_2\text{O}$ ratios less than 2. The K_2O and Na_2O contents vary from 3.5 to 5.5%, and 3.0 to 4.0%, respectively. Other oxides range from below: MgO (0.1 to 3%); CaO (1 to 4%); TiO_2 (0.05 to 0.8%) and $\text{Fe}_2\text{O}_{3\text{Total}}$ (1 to 5%).

In the Harker diagrams (Fig. 11), the compositional homogeneity of litotypes is better observed, therefore, the TiO_2 , CaO , P_2O_5 , MgO , and $\text{Fe}_2\text{O}_3(\text{t})$ diagrams present incipient negative correlation with increased SiO_2 , and positive with Na_2O for more evolved rocks. The trace elements show lesser compositional difference between the petrographic non-deformed types show that Rb and Ba behave compatibly since the contents decrease as silica increases, although they do not present continuous trends. The Sr content was directly proportional to the silica increase, in more evolved rocks, even with discontinuous trends. Y has a negative trend, decreasing for more developed rocks. Ga levels, on the other hand, show discontinuous trends that decreased in more evolved rocks. The Nb content displayed a discontinuous trend, decreasing with increasing silica, which is, decreasing in more evolved rocks.

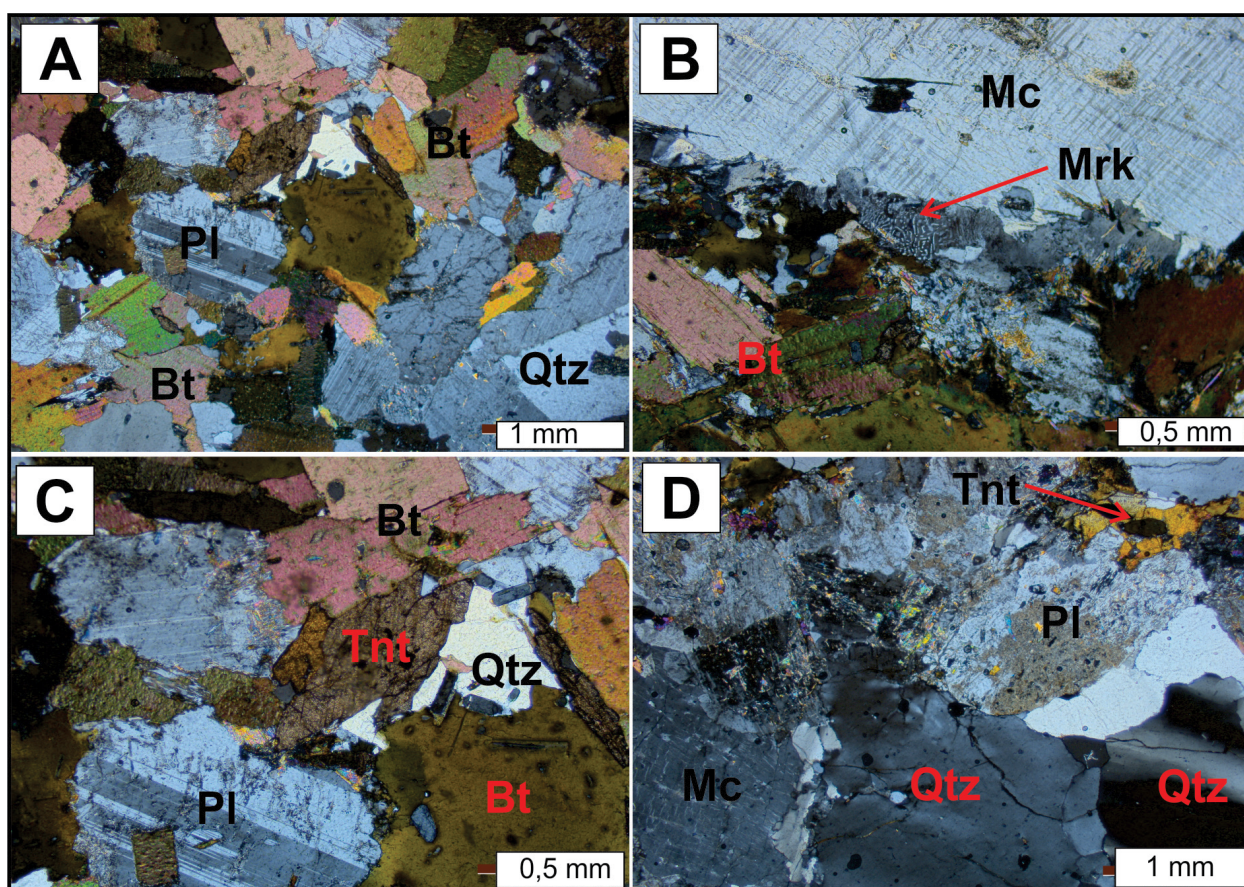


Figure 8. General petrographic aspects of the Magmatic Domain of the Chaval Granite: (A) Hipidiomorphic granular texture represented by plagioclase, quartz, microcline, biotite and titanite; (B) Part of the perthitic microcline megacrystal (top) involved in hipidiomorphic granular matrix. Note fine myrmekite intergrowths at the center photo (rede arrow); (C) Detail of euhedral titanite crystal associated with plagioclase and quartz. Note inclusions of apatite and zircon in biotite; (E) Ondulose extinction in quartz crystals representing incipient deformation. Mineral abbreviations according to Fettes and Desmons (2008).

The discriminant geochemical diagrams such as the R1-R2 classification (La Roche *et al.* 1980) show that most samples are located in the granodiorite field, whereas two samples (2011/CHA-29 and 2011/CHA-35) are in the tonalite field (Fig. 12). These geochemical behaviors are compatible with the petrographic classifications.

In the Shand alumina-saturation diagram (Fig. 13), most samples are observed in the peraluminous field grading to the metaluminous field, which is in agreement with the petrographic data in the presence of biotite, alkali-feldspar, and plagioclase.

In the AFM diagram, the samples lie below the dividing curve and clearly define a compositional trend compatible with the calcium-alkaline series (Fig. 14).

In the multi-element diagram normalized to the Thompson (1982) primitive mantle the samples show similar geochemical signatures, indicating co-geneticity with large ion light element (LILE) enrichment compared to the light rare earth elements (LREE) and high-field-strength elements (HFS), and negative Ba, Nb, P, and Ti anomalies, also reflecting the compositional variations (Fig. 15).

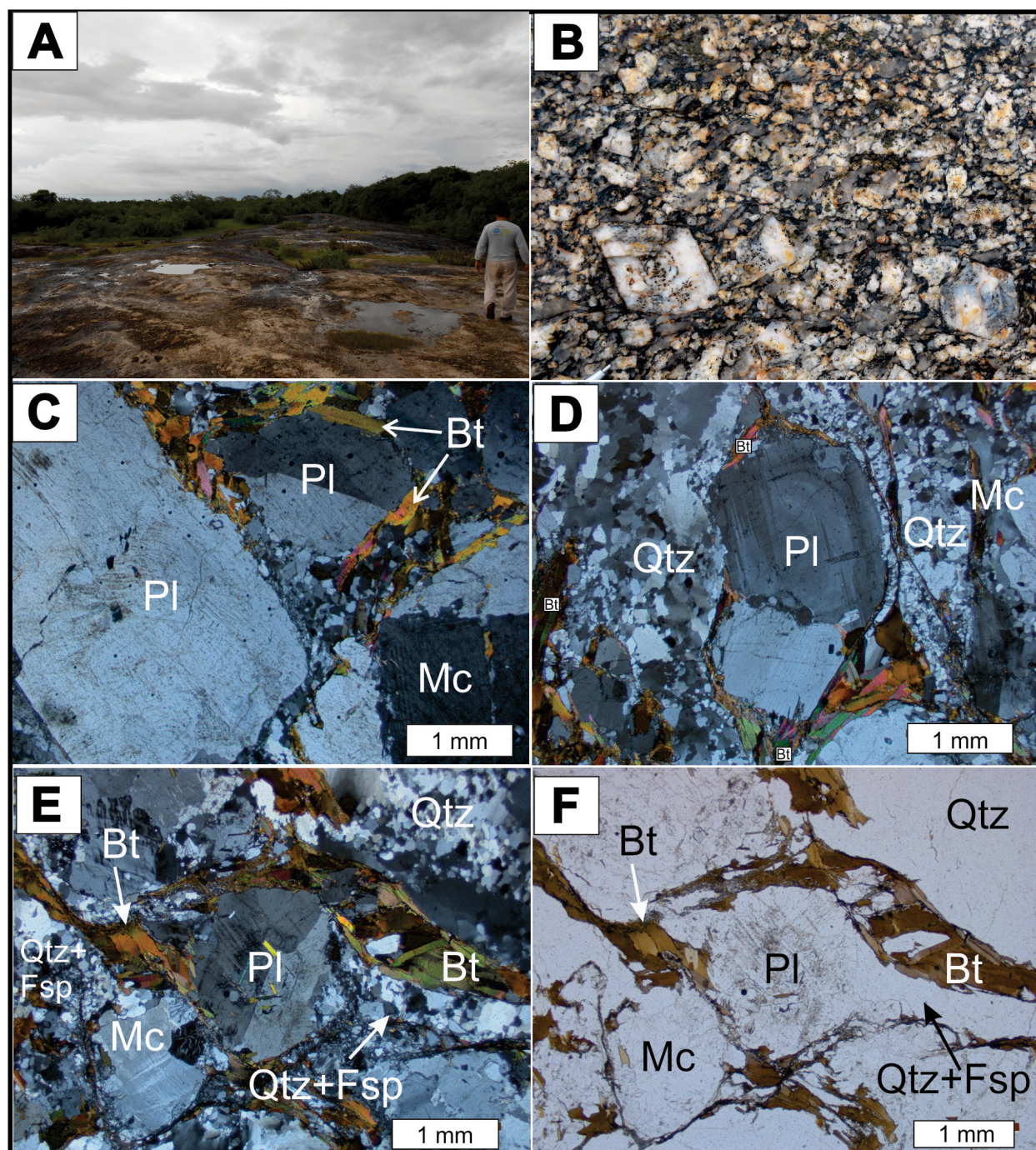


Figure 9. Representative images of the less deformed domain (protomylonite granites): (A) Large elongated outcrop of the Chaval Granite; (B) Centimetric microcline phenocrysts, slightly deformed, still preserving euhedral form and oscillatory zoning. Note deformation in the matrix of quartz and biotite with stretching, embriication minerals, and incipient foliation; (C) Protomylonite with partially preserved magmatic texture, with slight plagioclase phenocrystal deformation, in a fine quartz-feldspatic comminuted matrix with preferential orientation of biotite lamellae; (D) Preserved phenocrystal of plagioclase with magmatic zoning in deformed and recrystallized matrix. Note fine foliation of biotite and ribbon quartz surrounding the porphyroclasts; (E) Detail of plagioclase porphyroclastes ruptured and rotated in milonitic matrix, involved by biotite foliation; (F) Same D image of E, under natural light. Mineral abbreviations according to Fettes and Desmons (2008).

The behavior of rare earth elements (REE) also demonstrates this similarity by highlighting a slightly inclined pattern with enrichment of LREE compared to heavy rare earth elements (HREE), with moderate to high fractionation, with La/Yb ratio between 4.5 and 27, and moderate negative europium anomalies [(Eu/Eu*) N = 0.26 to 0.9] (Fig. 16).

In the granite typology diagrams of Whalen *et al.* (1987), the geochemical data are mostly in the field of I and S granites type, with some samples at the edge of this field (Fig. 17).

In the tectonic environment classification diagram by Pearce *et al.* (1984), the samples of the Chaval Granite plot in the field of granite magmatic arc, and according to Brown *et al.* (1984) are comparable to the Normal Continental Arc granites (Fig. 18). This allows linking the Chaval Granite emplacement to an orogenic environment related to the continental collision according to concepts of Pitcher (1993) and Barbarin (1999), and sin-collisional (Pearce *et al.*, 1984, Maniar and Piccoli, 1989).

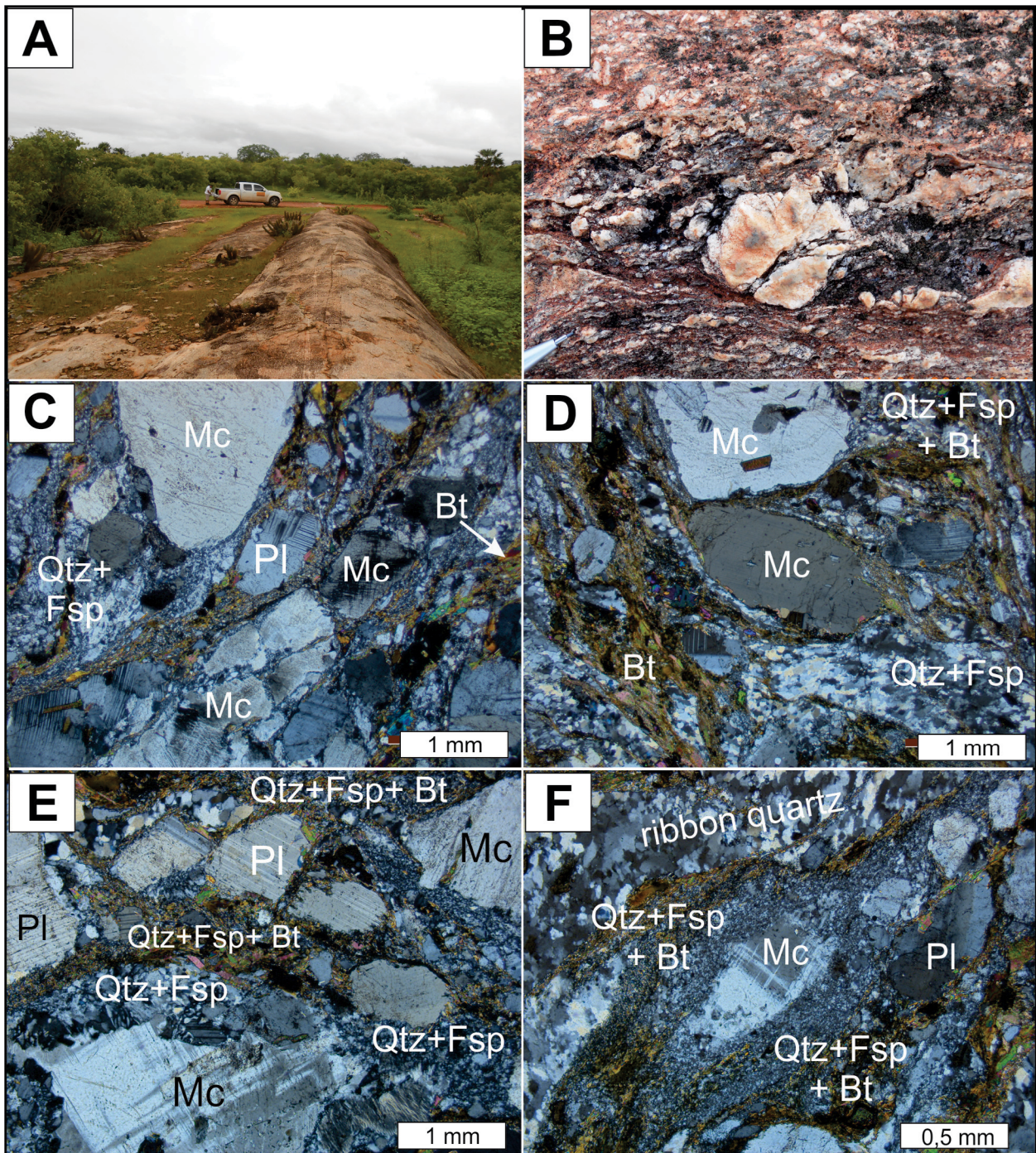


Figure 10. General features of milonitic granites: (A) Extensive elongated outcrop characteristic of mylonitic zones; (B) Porphyroblast of sigma-type alkaline feldspar, almond-shaped, immersed in a strongly comminuted and oriented matrix; (C) Microcline and plagioclase porphyroclasts with comminuted and recrystallized edges, with microfractures, in a polygonal granoblastic matrix; (D) Mylonitic anastomosed foliation formed by aligned biotite lamellae, ribbon quartz, and microcline porphyroclast stretched; (E) Microcline and plagioclase segmented porphyroclasts with comminuted edges, broken and rotated crystals, immersed in the fine comminuted granoblastic matrix; (F) Microcline strongly deformed, comminuted and recrystallized in fine polygonal grained matrix at the edges (core-mantle microstructure). Mineral abbreviations according to Fettes and Desmons (2008).

Table 2A. Geochemical analyzes of major, minor (weight %) and traces elements (ppm) of Chaval Granite.

SAMPLE	PROTOMILONITIC GRANITE				BIOTITA MONZOGRANITE	
	2010/CHA-01	2010/CHA-02	2010/CHA-03	2010/CHA-04	2010/CHA-10	2011/CHA-25
SiO ₂	70.78	70.66	68.14	70.32	64.99	69.57
TiO ₂	0.30	0.33	0.43	0.31	0.66	0.46
Al ₂ O ₃	14.65	14.66	15.28	15.02	14.60	14.65
Fe ₂ O ₃	2.79	2.91	4.02	2.96	4.61	2.98
MgO	1.02	1.07	1.41	1.03	2.54	0.96
CaO	1.88	1.85	1.95	1.87	3.24	2.26
MnO	0.06	0.06	0.07	0.06	0.08	0.04
Na ₂ O	4.12	4.07	3.85	4.21	2.61	3.42
K ₂ O	3.30	3.48	3.65	3.48	5.05	4.36
P ₂ O ₅	0.07	0.06	0.08	0.07	0.22	0.12
LOI	0.8	0.6	0.8	0.4	1.1	0.9
TOTAL	99.78	99.16	99.69	99.74	99.71	99.73
Ba	808.0	902.0	1422.0	862.0	1141.0	1033.0
Rb	94.2	90.9	91.5	93.8	224.2	130.7
Sr	880.7	897.2	974.6	889.3	353.2	560.9
Zr	93.0	90.8	151.1	91.9	209.8	181.0
Nb	6.6	6.7	7.3	6.7	16.4	9.7
Y	20.2	14.7	21.6	20.2	30.1	14.8
Ga	18.9	19.3	17.7	18.7	18.3	17.8
Ni	20	23.0	54.0	32.0	27.0	20
Ta	0.6	0.5	0.5	0.6	1.4	1.1
Th	4.3	3.2	5.5	4.0	23.4	15.4
Cs	5.7	4.5	5.1	5.1	9.9	5.1
Zn	54.0	53.0	57.0	57.0	54.0	56.0
U	1.7	1.2	1.4	1.7	6.5	2.0
V	40.0	43.0	61.0	41.0	76.0	40.0
La	15.1	14.7	27.5	14.8	52.0	45.2
Ce	31.9	29.7	54.3	28.9	109.4	83.2
Pr	3.63	3.37	6.02	3.33	13.09	9.05
Nd	12.9	13.3	22.9	13.8	53.3	34.2
Sm	2.8	2.3	4.0	2.8	9.9	5.2
Eu	0.6	0.7	1.1	0.7	1.8	1.1
Gd	2.9	2.4	3.4	2.9	7.3	3.4
Tb	0.52	0.40	0.58	0.50	1.14	0.51
Dy	3.2	2.4	3.5	2.9	6.3	2.7
Ho	0.73	0.47	0.79	0.67	1.07	0.42
Er	2.2	1.7	2.3	2.1	3.3	1.3
Tm	0.35	0.25	0.36	0.34	0.46	0.18
Yb	2.2	1.5	2.4	2.1	3.0	1.2
Lu	0.3	0.2	0.4	0.3	0.4	0.2
Σ REE	79.4	73.3	129.5	75.9	262.3	187.8
Na ₂ O + K ₂ O	7.42	7.55	7.50	7.69	7.66	7.78
K ₂ O/Na ₂ O	0.80	0.86	0.95	0.83	1.93	1.27
(La/Yb)N	4.57	6.61	7.76	4.84	11.84	25.39
Eu/Eu*	0.67	0.85	0.91	0.7	0.64	0.77
(La/Sm)N	3.37	3.99	4.36	3.31	3.31	5.45
(Gd/Yb)N	0.20	0.21	0.21	0.21	0.19	0.14

Table 2B. Geochemical analyzes of major, minor (weight %) and traces elements (ppm) of Chaval Granite.

AMOSTRA	BIOTITE GRANODIORITE			TONALITE		MILONITIC GRANITE	
	2010/CHA-06	2010/CHA-08	2011/CHA-27	2011/CHA-29	2011/CHA-35	2011/CHA-31	2011/CHA-13
SiO ₂	72.04	65.87	70.80	65.12	63.73	65.51	70.91
TiO ₂	0.29	0.83	0.36	0.68	0.66	0.82	0.29
Al ₂ O ₃	14.42	14.72	14.42	15.70	14.17	15.10	15.19
Fe ₂ O ₃	1.54	4.53	2.39	3.96	5.43	4.58	1.46
MgO	0.66	2.25	0.80	1.97	3.28	2.25	0.64
CaO	1.93	2.98	2.11	2.65	4.27	3.04	2.13
MnO	0.04	0.06	0.04	0.05	0.09	0.06	0.02
Na ₂ O	3.59	2.86	3.55	3.04	2.52	2.97	3.80
K ₂ O	4.48	4.51	4.37	5.46	4.19	4.50	4.49
P ₂ O ₅	0.07	0.25	0.10	0.20	0.32	0.23	0.08
LOI	0.8	0.9	0.8	0.9	1.0	0.7	0.8
TOTAL	99.86	99.77	99.74	99.74	99.68	99.77	99.81
Ba	819.0	682.0	1032.0	861.0	1413.0	668.0	577.0
Rb	166.9	241.8	138.5	234.2	187.3	237.2	242.7
Sr	467.7	303.7	532.1	325.8	502.6	296.8	469.9
Zr	107.6	288.7	127.3	248.8	199.5	278.4	123.4
Nb	8.8	19.4	9.2	14.7	11.4	18.6	8.0
Y	10.0	27.8	11.4	19.7	32.0	25.3	4.0
Ga	17.7	21.6	16.8	20.8	15.2	21.2	23.1
Ni	20	31.0	20	22.0	30.0	29.0	20
Ta	0.9	1.8	1.0	1.2	0.7	1.5	0.9
Th	25.3	27.2	12.9	20.5	21.3	25.3	9.4
Cs	5.6	12.3	5.8	7.3	8.1	12.4	25.7
Zn	36.0	70.0	43.0	62.0	46.0	74.0	41.0
U	3.4	3.9	2.0	2.5	3.5	3.6	3.3
V	18.0	66.0	30.0	54.0	91.0	65.0	16.0
La	41.7	71.5	32.0	55.6	54.5	68.5	21.7
Ce	75.8	144.7	63.8	111.8	112.3	139.4	42.9
Pr	7.87	17.36	6.92	12.95	13.37	16.56	4.82
Nd	27.2	66.2	25.0	48.5	51.3	65.2	19.0
Sm	4.0	11.6	4.5	8.7	9.0	11.0	2.9
Eu	0.8	1.6	1.0	1.4	1.9	1.5	0.7
Gd	2.4	8.1	2.9	6.0	7.1	8.0	1.7
Tb	0.35	1.15	0.44	0.87	1.07	1.13	0.20
Dy	1.8	5.7	2.2	4.4	6.0	5.5	0.9
Ho	0.35	0.98	0.37	0.75	1.21	0.97	0.13
Er	0.9	2.4	1.1	1.9	3.3	2.5	0.4
Tm	0.15	0.38	0.16	0.29	0.49	0.34	0.05
Yb	1.0	2.4	1.1	1.6	3.0	2.0	0.4
Lu	0.1	0.3	0.1	0.2	0.4	0.3	0.1
Σ REE	164.5	334.3	141.5	254.9	264.8	322.9	95.9
Na ₂ O + K ₂ O	8.07	7.37	7.92	8.50	6.71	7.47	8.29
K ₂ O/Na ₂ O	1.25	1.58	1.23	1.80	1.66	1.52	1.18
(La/Yb)N	27.56	20.51	20.35	23.88	12.46	23.56	34.02
Eu/Eu*	0.81	0.5	0.84	0.59	0.72	0.5	0.9
(La/Sm)N	6.56	3.87	4.45	4.03	3.8	3.92	4.64
(Gd/Yb)N	0.12	0.13	0.19	0.15	0.19	0.13	0.19

U-Pb GEOCHRONOLOGY

The ages of the Chaval Granite were determined by the U-Pb zircon dating technique, using the Thermo Finnigan Neptune Multi-collector mass spectrometer (ICP-MS-LA) in the Isotopic Geology Laboratory of the Geosciences Institute of the Federal University of Pará (Pará-Iso/IG, UFPA). The zircon grains were previously concentrated using conventional techniques, which included manual sifting in two fractions (250–180 and 180–125 μm), magnetic separation with neodymium magnet and Frantz Isodynamic apparatus, and gravimetric separation using the panning technique and micro-panning with 96° alcohol. The analytical procedures followed the recommendations of Ludwig (2003), Bühn *et al.* (2009), Chemale Jr. *et al.* (2012), and Milhomem Neto *et al.* (2017b). Cathodoluminescence images of the zircons were obtained using the scanning electron microscope (SEM) in the Microanalysis Laboratory of IG/UFPA.

The zircon grains were selected and fixed on cylindrical mounts in epoxy resin and later, polished to obtain a smooth surface. Subsequently, they were analyzed with a laser [New Wave UP 213 Nd: YAG ($\lambda = 213 \text{ nm}$)] coupled to a mass spectrometer (ICP-MS) at 10 Hz frequency, approximately 100 mJ/cm² energy and beam size between 15 and 30 μm. The instrumental mass differences were corrected using the GJ-1 standard zircon analysis (Jackson *et al.* 2004). The age calculations and the U-Pb data points were plotted in the Wetherill diagram using the ISOPLLOT/EX 3.0 software (Ludwig 2003).

For the geochronological studies, four samples of the Chaval Granite were selected and treated, two from the preserved

magmatic portion (2016-CHA-02 and 2016-CHA-05) and two from the deformed portion (2016-CHA-03 and 2016-CHA-12); however, only the two samples 2016-CHA-02 and 2016-CHA-05 produced satisfactory results.

The euhedral zircon crystals have well-defined faces, showing concentric magmatic zoning (Figs. 19 and 20).

The geochronological analysis results are displayed in Tables 3 and 4. Initially, the data show Th/U ratios between 0.15 and 1.0 for the majority analyzed zircon crystals, compatible

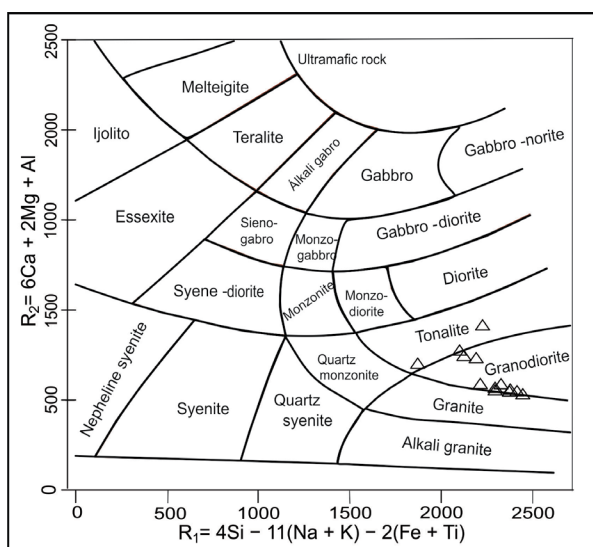


Figure 12. R1-R2 diagram of La Roche et al. (1980) with geochemical analyzes of the Chaval Granite.

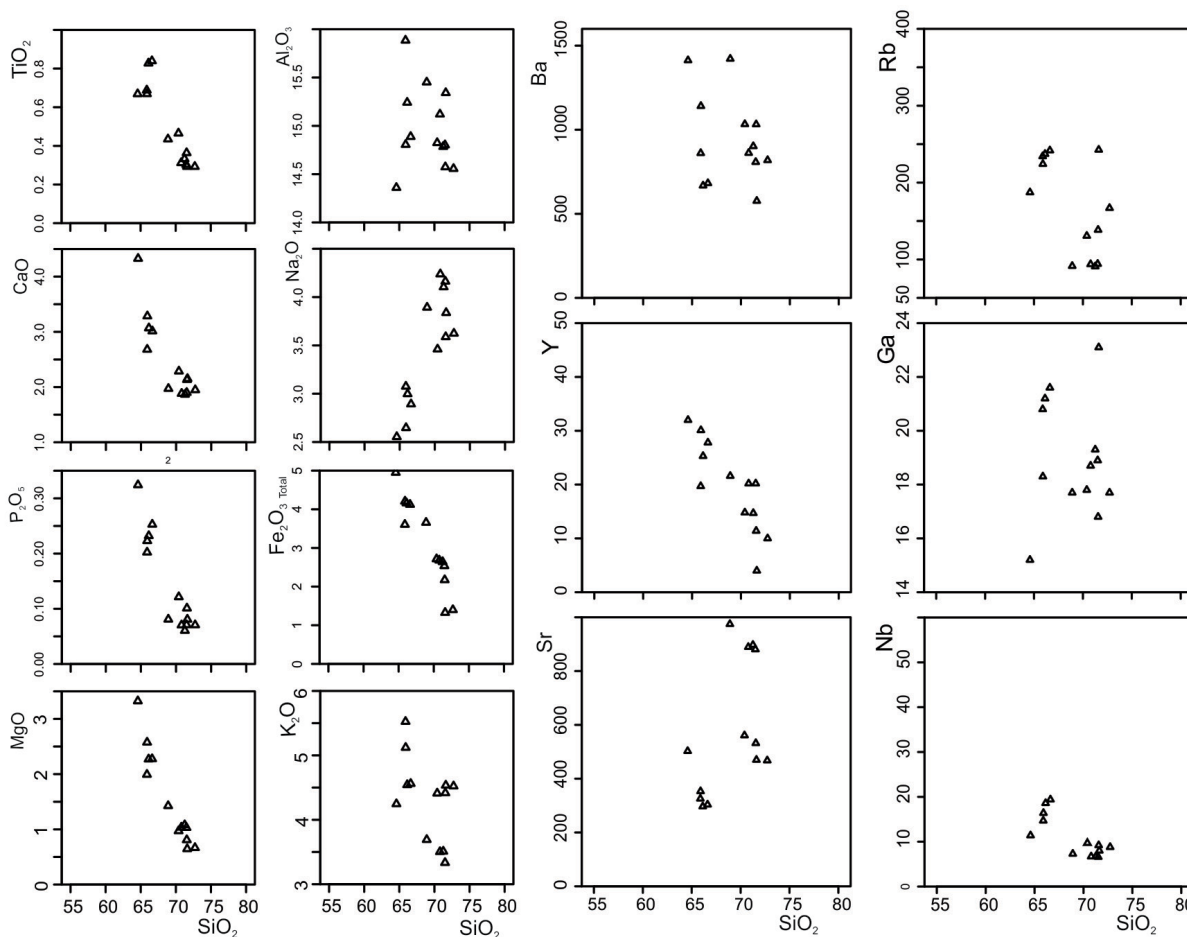


Figure 11. Harker diagrams for major (weight %) or trace (ppm) elements of Chaval Granite samples with data from Table 2.

with the magmatic zircon values ($Th/U > 0.1$) reported by Hoskin & Black (2000) and Rubatto (2002).

Thirty-three crystals from the 2016-CHA-02 sample were analyzed, and the isotopic data allowed calculating the discord line that resulted in a superior intercept age of 669 ± 68 Ma with $MSWD = 0.11$. However, only 18 zircon crystals defined a more accurate concordia age of 632.9 ± 8.3 Ma with $MSWD = 1.5$ (Fig. 21A), with a high degree of concordance and high analytical reliability. Thus, the age of 633 Ma is interpreted as representing the crystallization age of Chaval Granite.

Twenty-six crystal from the 2016/CHA-05 sample were analyzed, and the isotopic data allowed calculating the discord line that resulted in a superior intercept age of 528 ± 59 Ma with $MSWD = 0.79$. However, only 9 zircon crystals defined a more accurate concordia age of 633 ± 11 Ma with $MSWD = 0.00014$ (Fig. 21B). These data are similar to the other results and are interpreted as the age of crystallization for Chaval Granite.

Whole-rock Sm-Nd geochronology

Besides the crystallization age of the Chaval Granite, an isotopic study with the Sm-Nd - Model Age (T_{DM}) system was performed to determine the age of mantle separation/segregation from the original magma during the formation of the studied granite.

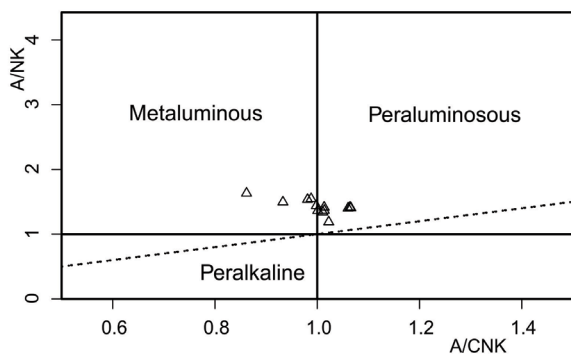


Figure 13. Geochemical diagram performed for the Chaval Granite, using Shand index classification of saturation in alumina (Shand 1950).

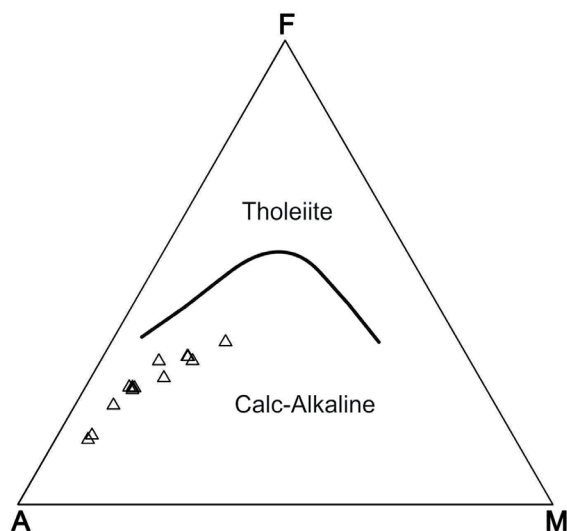


Figure 14. AFM diagram of magmatic series of Irvine and Baragar (1971) performed for the Chaval Granite.

The Sm-Nd isotopic analyses were performed in Pará-Iso Laboratory of Geoscience Institute/UFPA, following the analytical procedures of Gioia & Pimentel (2000) and Oliveira *et al.* (2008). Approximately 100 mg of pulverized rock was mixed with 100 mg of a $^{149}Sm-^{150}Nd$ Spike solution, which was dissolved in a Savillex vessel, using HNO_3 , HF , and HCl . The elements were extracted by two-stage ion-exchange chromatography on Teflon columns using the Eichron Ln resin for separation of Sm and Nd.

To correct mass discrepancies, the $^{143}Nd/^{144}Nd$ ratio was normalized to $^{143}Nd/^{144}Nd = 0.7219$, using the exponential law (Russel *et al.* 1978). The accuracy and reproducibility of the results were controlled based on the reference materials BCR-1, $^{143}Nd/^{144}Nd$, with a mean value ($n = 7$) of 0.512649 ± 12 (2σ) and La Jolla $^{143}Nd/^{144}Nd$ with a mean value ($n = 7$) of 0.511853 ± 5 (2σ). The decay constant used was $6.54 \times 10^{-12} a^{-1}$ according to Lugmair and Marti (1978) and the Nd model age (T_{DM}) was calculated according to the evolutionary mantle model of DePaolo (1981). During the Sm and Nd procedures, the chemical blanks were less than 0.1% of the concentrated element and were considered insignificant.

Whole-rock Sm-Nd data are listed in Table 5 and plotted in an $\epsilon_{Nd}(t)$ versus Age (Ma) evolution diagram (Fig. 22). The obtained values are acceptable for ratios $^{147}Sm/^{144}Nd$

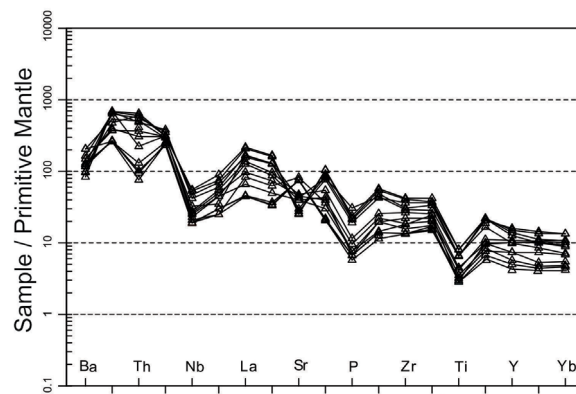


Figure 15. Multi elements diagrams normalized from the primitive mantle of Thompson (1982), for the Chaval Granite.

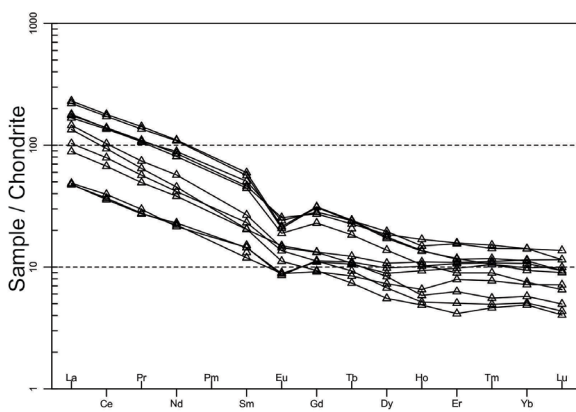


Figure 16. Distribution patterns of the REE normalized by chondrite of Boynton (1984) for representative samples of Chaval Granite.

(0.10202 to 0.12685) and degree of fractionation (-0.355 to -0.481), according to Sato and Tassinari (1997). The $\epsilon_{Nd}(t)$ values calculated according to the crystallization age obtained

in this work ($t = 633$ Ma), indicate negative values of -2.64, -8.06, and -9.13 and the calculated model ages (T_{DM}) indicate values of 1.27, 1.72, and 2.04 Ga.

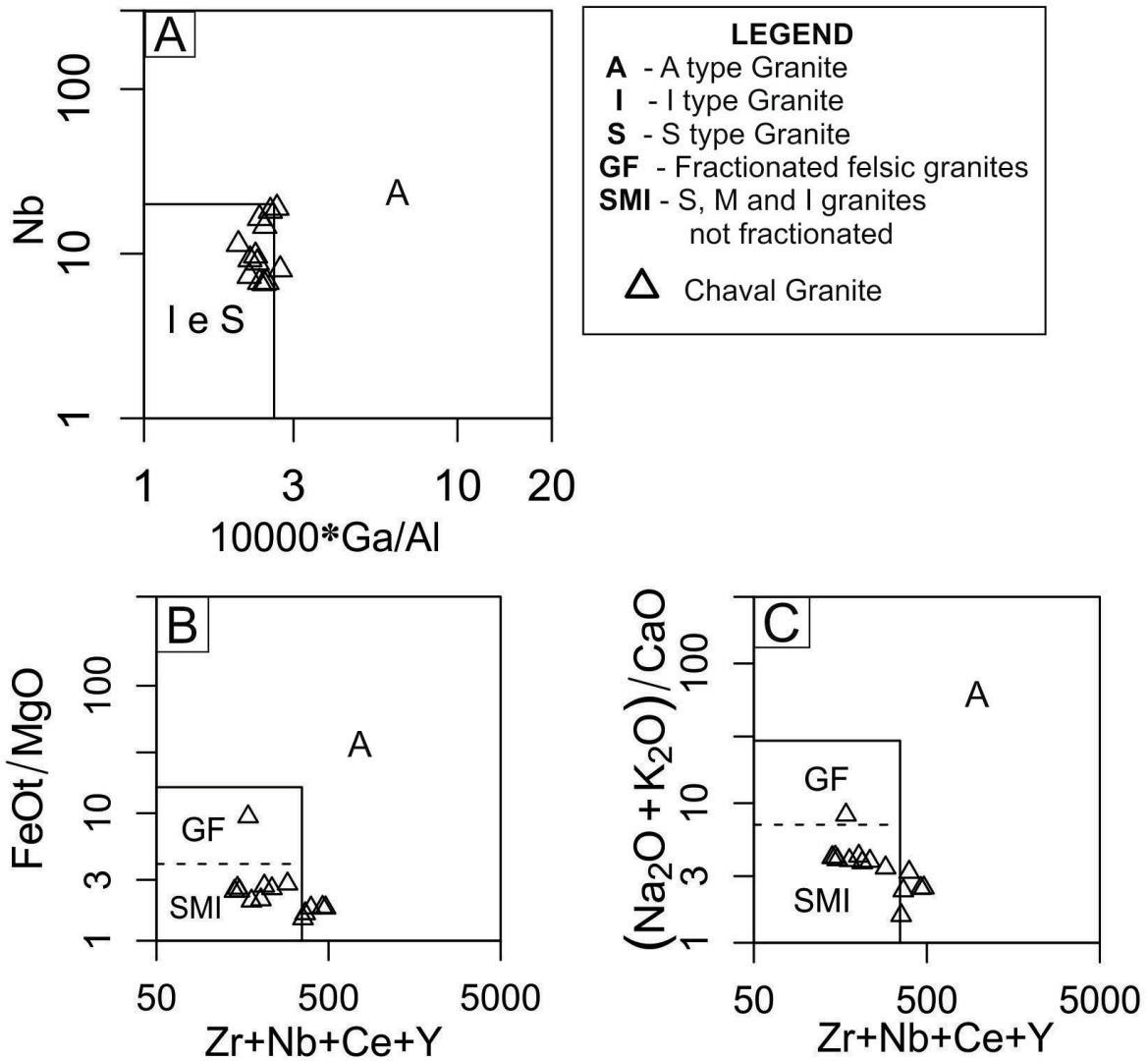


Figure 17. Geochemical diagram of granitoid typology of Whalen et al. (1987): (A) Nb versus $10,000 \times Ga / Al$; (B) Zr + Nb + Ce + Y versus FeOt / MgO; (C) $(Na_2O + K_2O) / CaO$ versus Zr + Nb + Ce + Y.

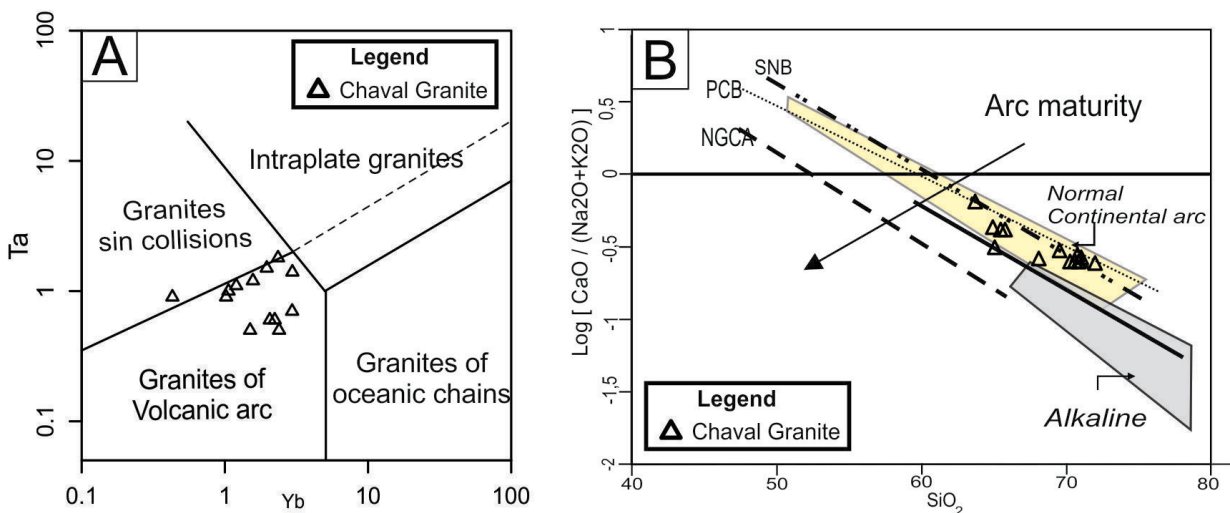


Figure 18. Geochemical discriminant diagrams of tectonic environments: (A) Y + Nb versus Rb, Pearce et al. (1984); (B) $\log [CaO / (Na_2O + K_2O)]$ versus SiO_2 , Brown et al. (1984).

In situ zircon Lu-Hf isotopes

Sample zircons (2016/CHA-02) were analyzed for Lu–Hf isotopes in domains with the same or similar internal structure to those analyzed for U–Pb dating. In this study, all the Hf isotopic measurements were performed on zircons with more than 95% of concordance on U–Pb ages. Initial $^{176}\text{Hf}/^{177}\text{Hf}$ ratios and $\epsilon_{\text{Hf}}(t)$ values were calculated for the respective U–Pb ages of the granitoids, using $t = 633$ Ma. The procedure of Hf analysis (Milhomem Neto *et al.* 2017a) was developed using a Neptune Thermo Finnigan multi-collector MC-ICP-MS coupled with an Nd:YAG 213 nm LSX-213 G2 CETAC laser microprobe. The laser spot used was 50 μm in diameter, with an ablation time of 60 s, a repetition rate of 10 Hz, and He used as the carrier gas. Mass bias corrections of Lu–Hf isotopic ratios were done by applying the variations of GJ-1 standard. The raw data were processed in Microsoft Excel worksheets to calculate the $^{176}\text{Hf}/^{177}\text{Hf}$ and $^{176}\text{Lu}/^{177}\text{Hf}$ ratios, the Hf model-age and $\epsilon_{\text{Hf}}(t)$ parameter for each analyzed point. The results are presented in Table 6. $\epsilon_{\text{Hf}}(t = 633 \text{ Ma})$ has been calculated using current chondritic uniform reservoir (CHUR)

values of $^{176}\text{Hf}/^{177}\text{Hf} = 0.282785$ and $^{176}\text{Lu}/^{177}\text{Hf} = 0.0336$ by Bouvier *et al.* (2008). $^{176}\text{Lu}/^{177}\text{Hf} = 0.0388$ and $^{176}\text{Hf}/^{177}\text{Hf} = 0.28325$ were used for depleted mantle (Andersen *et al.* 2009). $^{176}\text{Lu}/^{177}\text{Hf} = 0.015$ were used as the mean value of the continental crust to calculate the two-stage crustal Hf model age (Griffin *et al.* 2002, Belousova *et al.* 2009). Nine representative zircons of sample CHA-02 were analyzed. The results show variable $\epsilon_{\text{Hf}}(t = 633 \text{ Ma})$ values ranging from -9.6 to -18.1 and Hf crustal model ages from 2,131 to 2,653 Ma with an average age of ~ 2.32 Ga (Tab. 6, Fig. 23).

DISCUSSION AND FINAL CONSIDERATIONS

Field geological, geochronological and geochemical data allow us to conclude that the Chaval Granite occupies a vast outcrop area, featuring a batholith of more than 60 km wide, representing the most important magmatic body of the Northwest Ceará Domain. Its magmatic evolution with housing in plutonic conditions at medium crustal level may be related

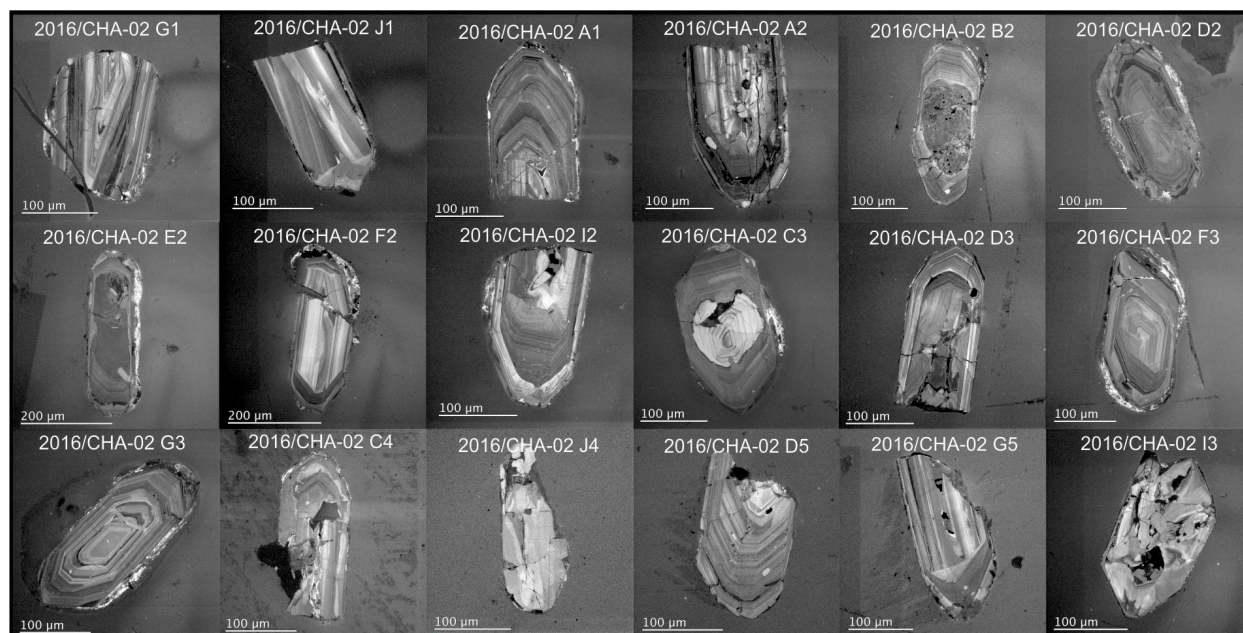


Figure 19. Cathodoluminescence zircon images from the 2016/CHA-02 sample, obtained by scanning electron microscope (SEM).

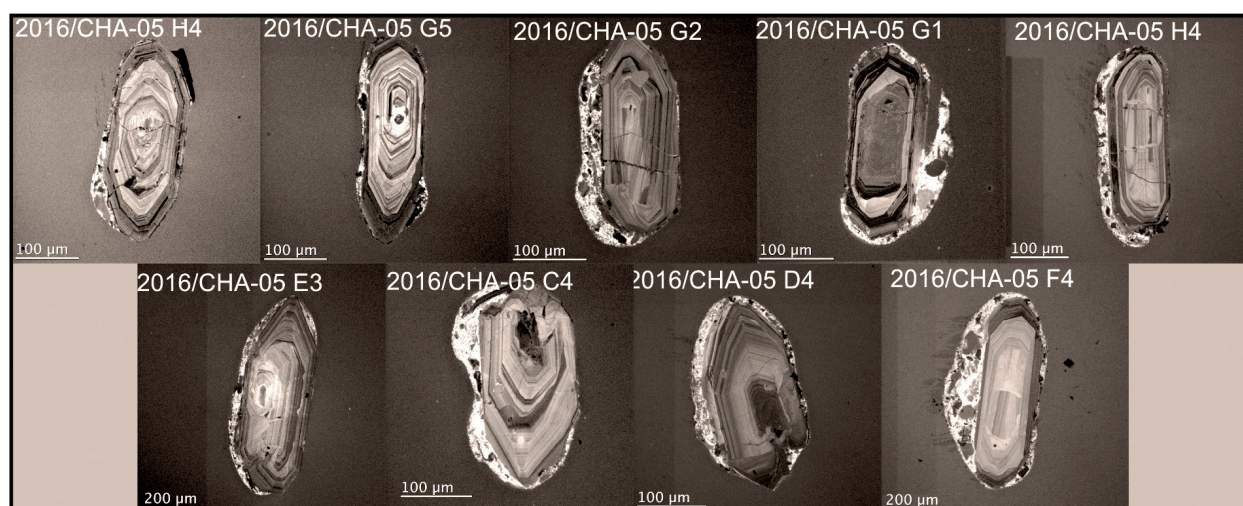


Figure 20. Cathodoluminescence zircon images from the 2016/CHA-05 sample, obtained by electron scanning microscope (SEM).

to a magmatic arc environment at the end of Neoproterozoic, whose southwest continuity hides under sedimentary cover (Parnaíba Block) (Brito Neves *et al.* 1984, Daly *et al.* 2014).

The results bring important advances to the geological knowledge of the region since it presents petrographic data associated to geochemical and isotopic data of U-Pb-Hf in zircon and Sm-Nd (T_{DM}) in whole-rock, previously unpublished in the literature.

The Chaval Granite is an atypical geological unit in the Northwest Ceará Domain, the northwestern edge of the Borborema Province, where it appears as an isolated body amidst the gneissic and supracrustal terrains of the Granja Complex and the Martinópolis Group, respectively.

The petrographic characteristics of plutonic nature and the deformational fabric imposed by the tectonics of the Santa Rosa Transcurrent Shear Zone are unique in the granitoids within this crustal domain and coincide with the data from Gorayeb & Lima (2014). On the other hand, there are similar and chrono-correlated granites in Ceará Central Domain, such as the granitoids of the Santa Quitéria Magmatic Arc.

The Chaval Granite has a predominantly monzogranitic and granodiorite composition, with tonalitic and syenitic

variations. However, despite its great extension, it is formed by very similar rocks, containing relatively homogeneous mineralogical associations (Mc, Pl, Qtz, and Bt). Structural, textural and microstructural aspects vary greatly throughout the body, defining a domain with preserved magmatic features to the northwestern portion of the body and other characterized by the presence of mylonitic features that are progressively more developed toward the eastern edge of the body, related to the edification of Santa Rosa Transcurrent Shear Zone.

The petrographic analysis, field data, petrography and literature suggest that the geological evolution of the Chaval Granite involved the accommodation of granite magma in orthogneisses of the Paleoproterozoic (Granja Complex) at middle crustal levels. This is suggested by the absence of thermal metamorphism, xenoliths, and chilled margins at the edges of the pluton, implying a low-temperature gradient between the magma and the country-rocks, as well as the ductile shear deformation conditions that affected the east flank of the body.

The evolution of Chaval Granite involved two main events. The first one comprises an important phase of the pluton emplacement involving magmatic differentiation that led to the formation of the main rocks of the body (porphyritic

Table 3 - U-Pb LA-MC-ICP zircon data for the sample 2016/CHA-02 (Chaval Granite).

Spot	f_{206}^a (%)	U ppm	Pb ppm	Th ppm	Th/U	$^{207}\text{Pb}/^{235}\text{U}$	Is (%)	$^{206}\text{Pb}/^{238}\text{U}$	Is (%)	rho	$^{207}\text{Pb}/^{206}\text{Pb}$	Is (%)	$^{206}\text{Pb}/^{238}\text{U}$ (Ma)	Is (abs)	$^{207}\text{Pb}/^{235}\text{U}$ (Ma)	Is (abs)	$^{207}\text{Pb}/^{206}\text{Pb}$ (Ma)	Is (abs)	Conc (%)
G1	1.74	223	31	220	0.99	0.888	9.75	0.103	4.10	0.42	0.062	2.64	633	26	645	63	688	18	98
J1	0.54	209	30	158	0.76	0.932	9.91	0.107	3.73	0.38	0.063	3.26	658	25	668	66	705	23	98
A1	0.37	564	69	132	0.24	0.943	9.84	0.111	4.24	0.43	0.062	2.50	676	29	675	66	670	17	100
A2	0.31	137	18	77	0.57	0.908	11.00	0.107	3.87	0.35	0.061	3.91	658	25	656	72	650	25	100
B2	0.47	445	56	124	0.28	0.895	7.12	0.102	2.19	0.31	0.064	2.81	625	14	649	46	734	21	96
D2	0.58	300	32	117	0.39	0.875	9.03	0.101	3.55	0.39	0.063	2.79	621	22	638	58	701	20	97
E2	2.29	215	38	59	0.28	0.840	6.34	0.101	2.00	0.31	0.060	2.46	619	12	619	39	620	15	100
F2	0.49	59	8	40	0.68	0.973	10.42	0.106	3.70	0.36	0.066	3.66	651	24	690	72	819	30	94
I2	0.59	417	39	69	0.17	0.856	6.40	0.100	2.68	0.42	0.062	1.76	612	16	628	40	686	12	97
C3	0.31	190	21	51	0.27	0.884	10.19	0.105	3.52	0.35	0.061	3.68	642	23	643	66	646	24	100
D3	0.48	542	56	92	0.17	0.911	9.38	0.102	3.91	0.42	0.065	2.59	624	24	658	62	776	20	95
F3	2.06	164	22	70	0.43	0.891	11.82	0.102	4.19	0.35	0.063	4.17	625	26	647	76	722	30	97
G3	2.09	528	59	197	0.38	0.867	6.72	0.103	2.27	0.34	0.061	2.47	631	14	634	43	644	16	100
C4	0.18	416	46	121	0.29	0.883	7.19	0.104	2.22	0.31	0.062	2.83	636	14	643	46	667	19	99
J4	0.45	185	30	28	0.15	0.873	10.41	0.102	3.01	0.29	0.062	4.25	627	19	637	66	672	29	98
D5	0.66	612	64	153	0.25	0.886	9.46	0.107	2.83	0.30	0.060	3.79	653	18	644	61	615	23	101
G5	0.44	371	40	79	0.22	0.920	7.10	0.106	2.52	0.35	0.063	2.50	649	16	662	47	707	18	98
I3	0.53	612	32	46	0.08	0.859	7.78	0.101	2.83	0.36	0.062	2.67	618	17	630	49	672	18	98
D1*	0.38	187	20	49	0.26	0.855	19.38	0.101	9.08	0.47	0.062	3.39	619	56	627	122	658	22	99
F1*	0.34	198	22	47	0.24	0.951	9.78	0.113	3.59	0.37	0.061	3.32	692	25	679	66	634	21	102
H1*	0.61	733	56	184	0.25	0.625	11.99	0.074	5.42	0.45	0.061	2.56	458	25	493	59	656	17	93
C1n*	0.36	79	7	64	0.82	0.634	28.91	0.070	11.85	0.41	0.066	8.28	433	51	499	144	811	67	87
C2*	0.37	278	28	75	0.27	0.788	11.30	0.092	4.63	0.41	0.062	3.24	568	26	590	67	675	22	96
G2*	2.29	82	14	38	0.46	0.993	12.96	0.117	3.91	0.30	0.061	5.17	714	28	700	91	656	34	102
H2*	2.50	373	50	286	0.77	0.798	11.02	0.094	4.39	0.40	0.062	3.34	579	25	595	66	657	22	97
B3*	0.21	227	28	78	0.35	0.946	7.94	0.112	2.65	0.33	0.061	2.96	685	18	676	54	646	19	101
J3*	1.86	491	38	155	0.32	0.809	30.49	0.093	15.03	0.49	0.063	2.54	574	86	602	184	709	18	95
E4*	0.40	299	28	81	0.27	0.697	8.75	0.082	3.19	0.36	0.062	3.00	507	16	537	47	665	20	94
H4*	0.55	162	20	154	0.95	0.886	16.91	0.097	3.93	0.23	0.067	7.49	594	23	644	109	823	62	92
I4*	0.50	523	54	148	0.29	0.765	8.83	0.088	3.54	0.40	0.063	2.63	544	19	577	51	709	19	94
I4n*	1.39	354	35	61	0.17	0.809	13.60	0.079	6.02	0.44	0.074	3.16	489	29	602	82	1053	33	81
C5*	0.33	83	14	37	0.46	0.904	21.07	0.110	9.14	0.43	0.059	5.24	674	62	654	138	585	31	103
I5*	0.27	576	53	136	0.24	0.717	23.19	0.085	11.21	0.48	0.061	2.94	524	59	549	127	655	19	95

^a Fraction of the non-radiogenic ^{206}Pb in the analyzed zircon spot, where $f_{206} = \frac{[^{206}\text{Pb}/^{204}\text{Pb}]_c}{[^{206}\text{Pb}/^{204}\text{Pb}]_s}$ (c: common; s: sample); *zircon excluded from the calculation of age.

monzogranites and granodiorites) in an important magmatic crystallization phase that generated the microcline megacrystals. In another phase, it involved the accumulation of microcline megacrystals (cumulative syenites), the formation of microdiorites by magma mixing, and late-stage aplites, leuco-alkaligranites, and pegmatites representing more advanced phases.

The initial phase is represented by the crystallization of plagioclase, biotite, and zircon, and then by alkali-feldspar (microcline megacrystals) under low nucleation and high growth rate

conditions, under low subcooling from the magma with significant hydration of the system (Paterson *et al.* 2005, Vernon 2008). This process was marked by successive stages of feldspar growth, as evidenced by the concentric zoning of the phenocrysts, which together with biotite represent an important phase of crystallization of the Chaval Granite, highlighted by the porphyritic texture with microcline megacrystals that continued with the oligoclase growth along with the microcline and, subsequently, the crystallization of quartz. Megacrystals

Table 4 - U-Pb LA-MC-ICP zircon data for the sample 2016/CHA-05 (Chaval Granite).

Spot	f_{206}^a (%)	U	Pb	Th	Th/U	$^{207}\text{Pb}/^{235}\text{U}$	Is		rho	$^{207}\text{Pb}/^{206}\text{Pb}$	Is		Is		Conc	Conc (%)			
		ppm	ppm	ppm			(%)	$^{206}\text{Pb}/^{238}\text{U}$			(%)	(abs)	$^{207}\text{Pb}/^{235}\text{U}$	(abs)			(Ma)		
H4	0.48	297.5	34.4	164.3	0.56	0.914	6.08	0.108	2.24	0.37	0.061	2.05	661	15	659	40	653	13	100
G5	0.20	303.5	36.5	87.7	0.29	0.934	11.47	0.111	4.97	0.43	0.061	2.86	677	34	670	77	646	18	101
G2	0.73	256.2	30.8	81.9	0.32	0.898	6.89	0.107	2.80	0.41	0.061	2.00	655	18	651	45	634	13	101
G1	0.72	122.3	15.9	83.4	0.69	0.838	7.16	0.096	2.70	0.38	0.063	2.35	590	16	618	44	722	17	95
E4	2.21	377.1	44.2	109.9	0.29	0.837	6.66	0.099	2.42	0.36	0.062	2.28	607	15	618	41	659	15	98
E3	2.16	223.5	30.9	116.9	0.53	0.844	8.10	0.099	3.17	0.39	0.062	2.52	611	19	621	50	659	17	98
C4	1.35	96.1	12.3	33.5	0.35	0.905	10.86	0.105	3.46	0.32	0.062	4.18	645	22	654	71	687	29	99
D4	1.13	76.8	9.9	29.1	0.38	0.849	5.83	0.105	2.14	0.37	0.059	1.98	641	14	624	36	562	11	88
F4	0.87	520.1	62.0	161.2	0.31	0.871	10.62	0.114	5.15	0.48	0.055	1.30	699	36	636	68	419	5	60
J1*	0.62	133.3	17.3	46.6	0.35	0.625	10.63	0.080	4.78	0.45	0.057	2.32	494	24	493	52	489	11	99
J2*	1.00	403.0	54.6	423.5	1.06	0.641	6.66	0.081	3.00	0.45	0.057	1.44	505	15	503	33	494	7	98
J3*	2.27	570.4	68.7	246.9	0.44	0.682	3.67	0.085	1.55	0.42	0.058	0.99	525	8	528	19	540	5	103
I5*	1.78	1481.4	160.0	607.7	0.41	0.645	3.59	0.079	1.15	0.32	0.059	1.38	489	6	505	18	577	8	118
I2*	0.35	465.0	63.5	207.4	0.45	0.753	4.28	0.089	1.87	0.44	0.061	1.05	552	10	570	24	641	7	116
I1*	1.00	247.6	34.1	65.7	0.27	0.631	6.87	0.084	2.79	0.41	0.055	2.01	519	14	497	34	396	8	76
H1*	0.66	202.0	22.8	68.0	0.34	0.742	4.87	0.091	1.87	0.38	0.059	1.56	562	10	564	27	572	9	102
H3*	0.05	105.3	11.8	43.9	0.42	0.596	6.44	0.075	2.24	0.35	0.057	2.31	469	10	475	31	505	12	108
J4*	0.54	2718.2	272.5	1784.5	0.66	0.712	10.93	0.083	4.96	0.45	0.062	2.30	513	25	546	60	687	16	94
I3*	0.15	598.9	63.5	207.4	0.35	0.751	12.91	0.088	5.62	0.44	0.062	3.18	546	31	569	73	663	21	96
F5*	0.30	372.9	40.7	90.0	0.24	0.665	4.61	0.088	1.77	0.38	0.055	1.48	541	10	518	24	415	6	77
E2*	0.41	429.6	34.6	90.0	0.21	0.737	6.19	0.093	2.80	0.45	0.058	1.31	572	16	561	35	513	7	90
F1*	1.56	222.4	27.2	135.3	0.61	0.779	6.70	0.092	2.80	0.42	0.061	1.83	568	16	585	39	651	12	97
E5*	0.62	61.8	6.7	19.2	0.31	0.773	20.05	0.092	6.89	0.34	0.061	7.28	566	39	582	117	643	47	97
D5*	0.64	322.8	45.2	129.5	0.40	0.662	3.87	0.088	1.32	0.34	0.054	1.41	546	7	516	20	383	5	70
E1*	0.35	62.5	7.6	14.4	0.23	0.801	7.77	0.109	1.60	0.21	0.053	3.54	670	11	597	46	332	12	50
G4*	3.15	262.9	19.0	80.4	0.31	0.807	4.41	0.106	1.14	0.26	0.055	1.89	652	7	601	26	411	8	63

^aFraction of the non-radiogenic ^{206}Pb in the analyzed zircon spot, where $f_{206} = [^{206}\text{Pb}/^{204}\text{Pb}]_c / [^{206}\text{Pb}/^{204}\text{Pb}]_s$ (c: common; s: sample); *zircons excluded from the calculation of age.

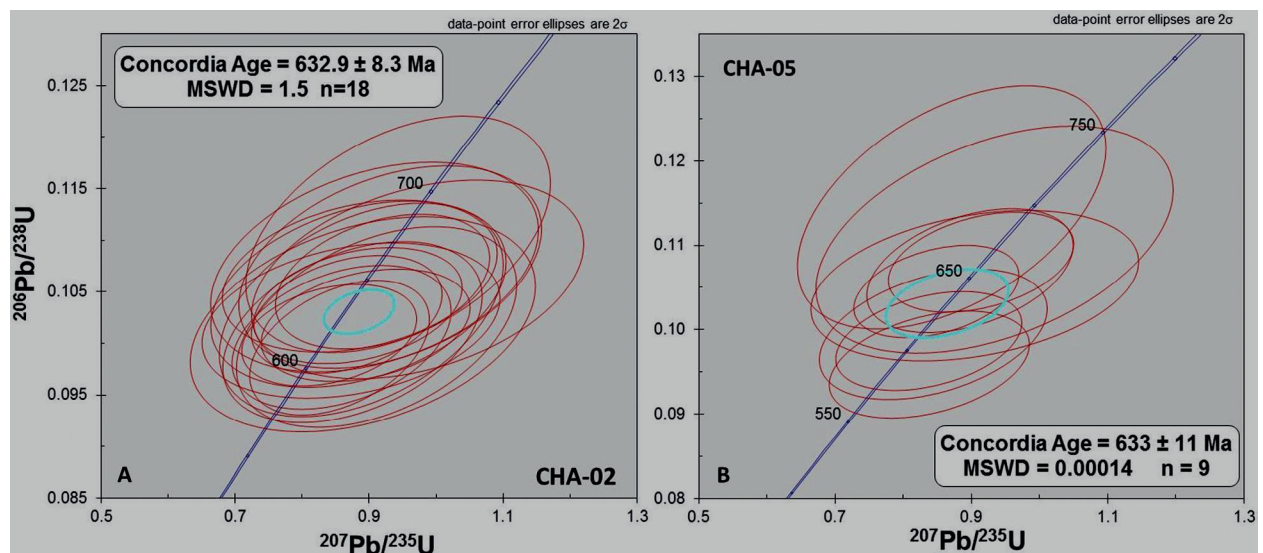


Figure 21. U-Pb concordia diagrams of samples (A) CHA-02 and (B) CHA-05 with LA-MC-ICP-MS zircon spot data and ages representing the age of emplacement of the Chaval Granite.

accumulation and magmatic layering flow structures are related to the process of magmatic differentiation and magma convection. Under these conditions, the phenocrysts tended to fluctuate in the residual magma in the magmatic chamber.

A remarkable characteristic of Chaval Granite is the presence of K-feldspar megacrystals, whose maximum dimensions reach 12 cm. The features indicate that these are crystals of magmatic origin, such as their euhedral forms, presence of simple twinning (Carlsbad), oscillatory normal zoning, plagioclase and biotite inclusions that delineate internal mineral growth zones and mixing of megacrysts into microdiorites enclaves.

Accumulations of K-feldspar megacrystals are frequent and prominent in the western pluton domain (region of Bom Princípio-PI), with much greater modal proportions (80 to 90%) in the coarse granitic matrix (residual magma). Normally, cumulates crystals are aligned denoting magmatic layering, with indicative of magma flows. Paterson *et al.* (2005) report a similar case in the Tuolumne Batholith of Sierra Nevada (California) where during K-feldspar growth, local mechanical instabilities in the magma were common and resulted in the physical accumulation of megacrysts in schlieren tubes, channels, irregular clusters, dike-like, and small diapirs. All of these features are identical to those reported in Chaval Granite.

In the later stages of tectonic evolution, after emplacement, an important deformational phase related to the SRTSZ formation, affecting all the east flank of the Chaval Granite and the ortogneisses country rocks. The rich and didactic collection of tectonic structures present in the eastern half of the pluton records the implantation of this shear zone with dextral kinematics, similar to those of the northern Borborema Province featuring a late Neoproterozoic transcurrent tectonic system (Arthaud & Torquato 1989), generated different mylonitic rocks (protomylonites, mylonites and ultramylonites).

The shearing process is related to the final stages of a continental collision formed in the final increments of the deformation

of an oblique collisional system that built the Northwest Ceará Shear Belt, leading to lateral extrusion of crustal masses in ductile flux at the end of the Brasiliano Orogeny in the northwest

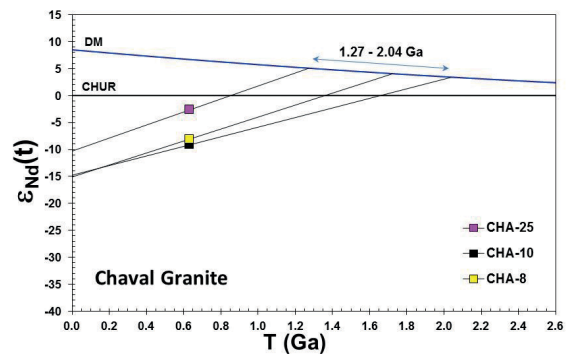


Figure 22. $\epsilon_{Nd}(t)$ versus age (Ga) diagram showing the evolution trends for the studied samples.

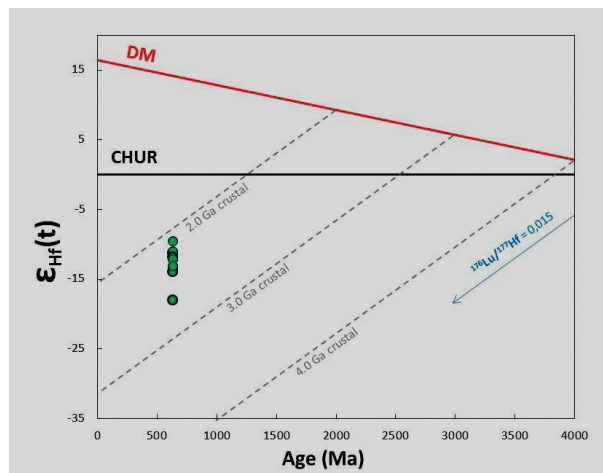


Figure 23. $\epsilon_{Hf}(t = 633 \text{ Ma})$ versus age (Ma) evolution diagram for the Chaval Granite. The dotted lines represent crustal evolution trends, calculated using $^{176}\text{Lu}/^{177}\text{Hf}$ of 0.015 for the average continental crust. (Griffin *et al.*, 2002).

Table 5 - Whole-rock ID-TIMS Sm-Nd isotope composition of samples of the Chaval Granite.

Sample	Sm (ppm)	Nd (ppm)	$^{147}\text{Sm}/^{144}\text{Nd}$	$^{143}\text{Nd}/^{144}\text{Nd} (\pm 2s)$	$f_{\text{Sm}/\text{Nd}}$	$e_{\text{Nd}}(0)$	$e_{\text{Nd}}(t=633 \text{ Ma})$	$T_{\text{DM}} (\text{Ga})$
CHA-25	5.04	29.86	0.10202	0.512110 (10)	-0.481	-10.30	-2.64	1.27
CHA-08	11.11	61.32	0.10958	0.511864 (08)	-0.443	-15.10	-8.06	1.72
CHA-10	9.89	47.12	0.12685	0.511881 (11)	-0.355	-14.77	-9.13	2.04

Table 6 - LA-MC-ICP-MS Lu-Hf isotope data of zircon for Chaval Granite (sample CHA-02).

Spot	$^{176}\text{Hf}/^{177}\text{Hf}_{\text{zircão}}$	2SE	$^{176}\text{Lu}/^{177}\text{Hf}_{\text{zircão}}$	2SE	$\epsilon_{\text{Hf}}(0)$	$t_{(\text{U-Pb})} (\text{Ma})$	$^{176}\text{Hf}/^{177}\text{Hf}_{(t)}$	$\epsilon_{\text{Hf}}(t)$	$T_{\text{DM}}^c (\text{Ma})^*$
A1	0.282072	0.000046	0.000432	0.000038	-25.2	633	0.282066	-11.3	2234
A2	0.282017	0.000077	0.000705	0.000087	-27.2	633	0.282008	-13.4	2361
G1	0.282123	0.000074	0.000815	0.000016	-23.4	633	0.282114	-9.6	2131
D2	0.282082	0.000072	0.000604	0.000029	-24.9	633	0.282074	-11.0	2217
E2	0.282054	0.000087	0.000455	0.000014	-25.9	633	0.282048	-11.9	2274
F2	0.281992	0.000108	0.000114	0.000080	-28.0	633	0.281991	-14.0	2400
I2	0.282047	0.000090	0.000419	0.000024	-26.1	633	0.282042	-12.2	2288
D3	0.282024	0.000093	0.000812	0.000042	-26.9	633	0.282015	-13.1	2347
F3	0.281875	0.000101	0.000120	0.000006	-32.2	633	0.281874	-18.1	2653

*Two-stage crustal model age (T_{DM}^c) using the respective U-Pb age and a $^{176}\text{Lu}/^{177}\text{Hf} = 0.015$ for the average continental crust (Griffin *et al.* 2002).

of the Borborema Province (Abreu *et al.* 1989, Arthaud & Torquato 1989, Ganade de Araujo *et al.* 2013).

During deformation, the primary mineral phases were transformed or re-equilibrated to the new P-T parameters, which in the general context indicate that there is a gradation of dynamic metamorphism, increasing from west to east, since non-metamorphosed and undeformed granitic rocks (location Bom Princípio), followed by low-grade areas (paragenesis Qtz-Sc-Ep-Chl) and finally, at the eastern end, with stabilization of the Kfs-Pl-Bt-Qtz paragenesis that reaches the maximum conditions of dynamic metamorphism in amphibolite facies, as described by Gorayeb & Lima (2014).

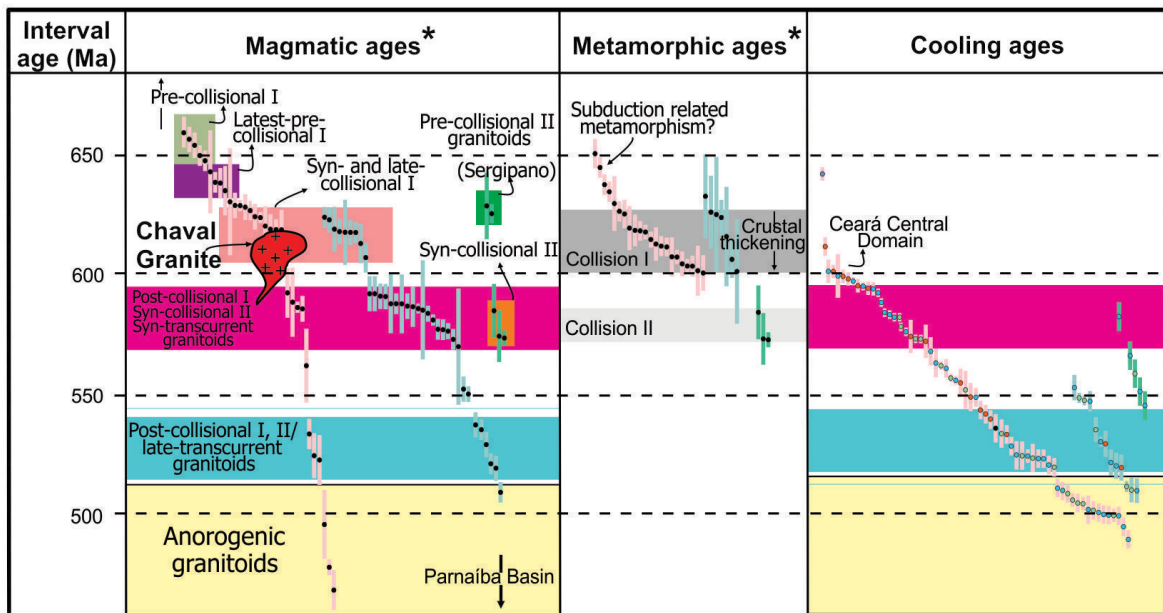
The varied types of mylonitic rocks formed and the structural/microstructural features identified are classic and similar to those described by Sibson (1977), White *et al.* (1980), Lister & Snoke (1984), Passchier and Trouw (1998), and Trouw *et al.* (2010). Based on the proposed classification of mylonites by Trouw *et al.* (2010) we can fit into the type of mid-grade mylonite.

The geochemical data reveal a systematic compositional variation, defining trends related to magmatic differentiation, with varying granodiorites, monzogranites, and tonalites, and of I-type and peraluminous to metaluminous character, compatible with the calcium-alkaline series. All these characteristics and the data in the discriminant diagrams of the tectonic environment reveal that the Chaval Granite is compatible with a normal type magmatic arc environment.

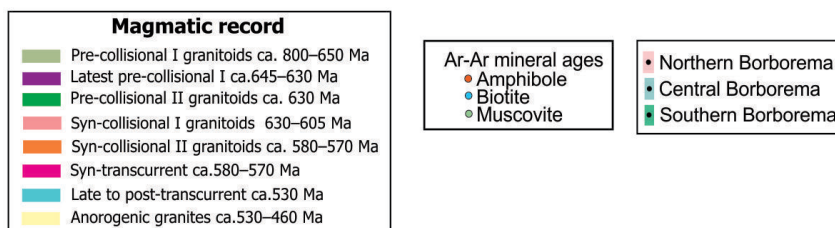
The geochronological studies in the literature pointed ages U-Pb on monazite crystals of 591 ± 10 Ma (Fetter 1999); and Pb evaporation in zircon 630 ± 19 Ma (Lima 1997) and 633 ± 3 Ma (Nogueira *et al.* 2013). The geochronological results of the U-Pb zircon systematic (U-Pb/LA-ICP-MS) indicate a crystallization age of 633 Ma for the Chaval Granite. This value is much more representative than other existing data in the literature and coincides with the preliminary dates obtained by Pb evaporation, indicating that the Chaval Granite emplacement occurred at the end of the Neoproterozoic, during the Cryogenian-Ediacaran period. Similar ages, between 624 and 666 Ma, have been determined in granitoids that integrate the Tamboril-Santa Quitéria Complex (Santa Quitéria Magmatic Arc) in the north region of the Borborema Province (Cavalcante *et al.* 2003, Fetter *et al.* 2003, Ganade de Araujo *et al.* 2013, 2014) (Fig. 24). Correlating with the evolutionary framework of Ganade de Araujo *et al.* (2013) the Chaval Granite fits into the tectonic context of syn-tardi collisional granite.

The 633 Ma Chaval Granite show Hf crustal model ages of 2.65 to 2.13 Ga. This indicates that the Chaval Granite incorporated Neoproterozoic and Paleoproterozoic crustal components during their genesis. The $\epsilon_{\text{Hf}}(t)$ values ranging from -9.6 to -18.1 suggest a long crustal residence time. These strongly negative values of $\epsilon_{\text{Hf}}(t)$ highlight the character of rocks associated with the partial melting of Neoproterozoic to Paleoproterozoic continental crust.

Whole-rock ID-Tims Sm-Nd isotopic study, shows significantly smaller data, though similar, to Lu-Hf data, T_{DM}



* Ages from anatectic crustal granitoids are considered both as metamorphic and magmatic.



Source: adapted from Ganade de Araujo *et al.* (2013).

Figure 24. Schematic chart with temporal and spatial distribution of the main granitoids of Borborema Province with Chaval Granite positioning and correlation.

model ages of 2.04, 1.72 and 1.27 Ga, with negative $\epsilon_{Nd}(t)$ values (-2.64 to -9.13), indicating contributions from paleoproterozoic and mesoproterozoic sources, with a considerable time of crustal residence that implies a more advanced (or mature) nature.

These ages are recognized in the literature as related to a succession of emplacement pulses that make up the Santa Quitéria Magmatic Arc (SQMA). The fact that Chaval Granite can be correlated to SQMA, indicates that its most distal portion is over 100 km NW from this arc. In the region, only granitoids related to the Tamboril-Santa Quitéria Complex have similar values, ranging from 637 to 624 Ma and 638 Ma for porphyritic monzogranites of the Santa Quitéria unit.

ARTICLE INFORMATION

Manuscript ID: 20190089. Received on: 09/10/2019. Approved on: 02/27/2020.

A. A. acted in all phases of research development, from fieldwork to the conception of the first version of the scientific article; elaborated the figures and tables, whose data come from his Master thesis. He performed laboratory work including petrographic analysis, sample preparation for geochronological studies. M. G. participated in the treatment, calculation and interpretation of geochronological data; wrote the topic on the Lu-Hf isotopic geology. P. G. acted as advisor and research coordinator as well as in the article integration data, discussion and interpretation on the structural, tectonics and petrological topics; carried out the samples and geochemical analyzes and petrological discussion of these data. He performed the translation into English, revised the article in its various versions, considering the recommendations of the reviewers. He integrated the text by elaborating new topics and rewrote the discussion and conclusive topics. He reworked the figures in the article.

Competing interests: The authors declare no competing interests.

REFERENCES

- Abreu F.A.M., Gama Jr. T.G., Gorayeb P.S.S., Hasui Y. 1988. O Cinturão de Cisalhamento Noroeste do Ceará. In: Congresso Latino-Americano de Geologia, 7., Belém. *Anais...*, v. 1, p. 20-34.
- Abreu F.A.M., Gorayeb P.S.S., Gama Jr. T. 1989. Aspectos tectônicos da região de Martinópolis-Massapê-CE. In: Simpósio de Geologia do Nordeste, 13., Fortaleza. *Anais...*, p. 265-267.
- Almeida C.N., Guimarães I.P., Silva Filho A.F. 2002. Petrogênese de rochas plutônicas félsicas e máficas na Província Borborema, NE do Brasil: o complexo cálcio alcalino de alto-K de Campina Grande. *Revista Brasileira de Geociências*, **32**(2):205-216.
- Amaral W.S., Santos T.J., Ancelmi M.F., Fuck R.A., Dantas E.L., Matteini M., Moreto C.P. 2015. 1.57 Ga protolith age of the Neoproterozoic Forquilha eclogites, Borborema Province, NE-Brazil, constrained by U-Pb, Hf and Nd isotopes. *Journal of South American Earth Sciences*, **58**:210-222. <https://doi.org/10.1016/j.jsames.2014.10.001>
- Andersen T., Andersson U.B., Graham S., Aberg G., Simonsen S.L. 2009. Granitic magmatism by melting of juvenile continental crust: new constraints of the source of paleoproterozoic granitoids in Fennoscandia from Hf isotopes in zircon. *Journal of the Geological Society*, **166**:233-247.
- Archanjo C.J., Launeau P., Hollanda M.H.B.M., Macedo J.W.P., Liu D. 2009. Scattering of magnetic fabrics in the Cambrian alkaline Meruoca Granite (Ceará State, northeastern Brazil). *International Journal of Earth Sciences*, **98**(8):1793-1807. <https://doi.org/10.1007/s00531-008-0342-z>
- Arthaud M.H. 2007. *Evolução neoproterozoica do Grupo Ceará (Domínio Ceará Central, nordeste do Brasil): da sedimentação à colisão continental brasileira*. Tese (Doutorado), Universidade de Brasília, Brasília, 132 p.
- Arthaud M.H., Torquato J.R. 1989. A tectônica transcorrente no estado do Ceará. In: Simpósio Nacional de Estudos Tectônicos, 2., Fortaleza. *Anais...*, p. 277-278.
- Barbarin B. 1999. A review of the relationships between granitoid types, their origins and their geodynamic environments. *Lithos*, **46**:605-626.
- Bell T.H., Etheridge M.A. 1973. Microstructures of mylonites and their descriptive terminology. *Lithos*, **6**(4):337-348. [https://doi.org/10.1016/0024-4937\(73\)90052-2](https://doi.org/10.1016/0024-4937(73)90052-2)
- Belousova E.A., Reid A.J., Griffin W.L., Suzanne Y. O'Reilly. 2009. Rejuvenation vs. recycling of Archean crust in the Gawler Craton, South Australia: Evidence from U-Pb and Hf isotopes in detrital zircon. *Lithos*, **113**:570-582.
- Bizzi L.A., Schobbenhaus C., Vidotti R.M., Gonçalves J.H. 2003. *Geologia, tectônica e recursos minerais do Brasil: texto, mapas & SIG*. Brasília, CPRM, 692 p.
- Bouvier A., Vervoort J.D., Patchett P.J. 2008. The La-Hf and Sm-Nd isotopic composition of CHUR: constraints from unequilibrated chondrites and implications for the bulk composition of terrestrial planets. *Earth and Planetary Science Letters*, **273**:48-57.
- Boynton W.V. 1984. Cosmochemistry of the rare-earth elements: meteorite studies. In: Henderson P. (ed.), *Rare-earth elements geochemistry*. Amsterdam, Elsevier, p. 63-114.
- Brito Neves B.B., Fuck R.A., Cordani U.G., Thomas Filho A. 1984. Influence of basement structures on the evolution of the major sedimentary basins of Brazil: a case of tectonic heritage. *Journal of Geodynamics*, **1**(3-5):495-510. [https://doi.org/10.1016/0264-3707\(84\)90021-8](https://doi.org/10.1016/0264-3707(84)90021-8)
- Brito Neves B.B., Santos E.J., Van Schmus W.R. 2000. Tectonic history of the Borborema province, northeastern Brazil. In: International Geological Congress, 31., Rio de Janeiro. *Anais...*, p. 151-182.
- Brito Neves B.B., Van Schmus W.R., Fetter A.H. 2001. Noroeste da África - Nordeste do Brasil (Província Borborema) Ensaio corporativo e problemas de correlação. *Geologia Série Científica USP*, **1**:59-78. <https://doi.org/10.5327/S1519-874X2001000100005>
- Brown G.C., Thorpe R.S., Webb P.C. 1984. The geochemical characteristics of granitoids in contrasting arcs and comments on source magmas. *Journal of Geological Society*, **141**:413-426. <https://doi.org/10.1144/gsjgs.141.3.0413>
- Bühn B., Pimentel M.M., Matteini M., Dantas E.L. 2009. High spatial resolution analysis of Pb and U isotopes for geochronology by laser ablation multi-collector inductively coupled plasma mass spectrometry (LA-MC-ICP-MS). *Anais da Academia Brasileira de Ciências*, **81**(1):99-114. <https://doi.org/10.1590/S0001-37652009000100011>

ACKNOWLEDGMENTS

This study was conducted by the research group "Petrology and Crustal Evolution" (CNPq-UFPA) within the scope of the Graduate Program in Geology and Geochemistry (PPGG), Geosciences Institute (IG) of the Federal University of Pará (UFPA). Thanks to the Isotope Geology Laboratory (Pará-Iso) -IG-PPGG for isotope analyzes and the IG/PPGG for the infrastructure. We are also grateful to the Microanalyses Laboratory for capturing images of catodoluminescence acquired in scanning electron microscopy (SEM). The first author would like to thank the Coordination for the Improvement of Higher Education Personnel (CAPES) for the grant of the Master's scholarship.

- Cavalcante J.C., Vasconcelos A.M., Medeiros M.F., Paiva I.P., Gomes F.E.M., Cavalcante S.N., Cavalcante J.E., Melo A.C.R., Duarte Neto V.C., Bevenides H.C. 2003. *Mapa Geológico do Estado do Ceará*. Escala 1:500.000. Fortaleza, CPRM.
- Chemale Jr. F., Kawashita K., Dussin I.A., Ávila J.N., Justino D., Bertotti A. 2012. U-Pb zircon in situ dating with LA-MC-ICP-MS using a mixed detector configuration. *Anais da Academia Brasileira de Ciências*, **84**(2):275-296. <https://doi.org/10.1590/S0001-37652012005000032>
- Costa M.J., França J.B., Lins C.A.C., Bacchiegga I.F., Habekost C.R., Cruz W.B. 1979. *Geologia da Bacia de Jaibaras, Ceará, Piauí e Maranhão – Projeto Jaibaras*. Brasília, MME/DNPM, Série Geologia Básica 11, 106 p.
- Daly M.C., Andrade V., Barousse C.A., Costa R., McDowell K., Piggott N., Poole A.J. 2014. Brasileiro crustal structure and the tectonic setting of the Parnaíba basin of NE Brazil: results of a deep seismic reflection profile. *Tectonics*, **33**(11):2102-2120. <https://doi.org/10.1002/2014TC003632>
- Danni J.C.M. 1972. Geologia da porção sul do Grupo Jaibaras, *Revista Brasileira de Geociências*, **2**:85-97.
- DePaolo D.J. 1981. A neodymium and strontium isotopic study of the Mesozoic calcalkaline granitic batholiths of the Sierra Nevada and Peninsular Ranges, California. *Journal of Geophysical Research*, **86**(B11):10470-10488. <https://doi.org/10.1029/JB086iB11p10470>
- Ferreira V.P., Sial A.N., Jardim De Sá E.F. 1998. Geochemical and isotopic signatures of Proterozoic granitoids in terranes of the Borborema structural Province, northeast Brazil. *Journal of South American Earth Sciences*, **11**(5):439-455. [https://doi.org/10.1016/S0895-9811\(98\)00027-3](https://doi.org/10.1016/S0895-9811(98)00027-3)
- Fetter A.H. 1999. *U/Pb and Sm/Nd geochronological constraints on the crustal framework and geologic history of Ceará State, NW Borborema Province, NE Brazil: Implications for the assembly of Gondwana*. Tese (PhD), University of Kansas, Kansas, 164 p.
- Fetter A.H., Santos T.J.S., Van Schmus W.R., Hackspacher P.C., Brito Neves B.B., Arthaud M.H., Nogueira Neto J.A.A., Wernick E. 2003. Evidence for Neoproterozoic Continental Arc Magmatism in the Santa Quitéria Batholith of Ceará State, NW Borborema Province, NE Brazil: Implications for the Assembly of West Gondwana. *Gondwana Research*, **6**(2):265-273. [https://doi.org/10.1016/S1342-937X\(05\)70975-8](https://doi.org/10.1016/S1342-937X(05)70975-8)
- Fetter A.H., Van Schmus W.R., Santos T.J.S., Nogueira Neto J.A., Arthaud H.M. 2000. U-Pb and Sm-Nd geochronological constraints on the crustal evolution and basement architecture of Ceará state, NW Borborema province, NE Brazil: implications for the existence of the Paleoproterozoic supercontinent Atlantica. *Revista Brasileira de Geociências*, **30**(1):102-106.
- Fettes D., Desmons J. 2008. *Metamorphic rocks: a classification and glossary of terms*. Cambridge, Cambridge University Press, 244 p.
- Gama Jr. T., Gorayeb P.S.S., Abreu F.A.M. 1988. O Granito Pedra do Sal e suas feições de cisalhamento. *Revista Brasileira de Geociências*, **18**(4):424-432.
- Ganade de Araujo C.E., Cordani U.G., Weinberg R., Basei M.A.S., Armstrong R.A., Sato K. 2014. Tracing Neoproterozoic subduction in the Borborema Province (NE, Brazil): clues from U–Pb geochronology and Sr–Nd–Hf–O isotopes on granitoids and migmatites. *Lithos*, **202-203**:167-189. <https://doi.org/10.1016/j.lithos.2014.05.015>
- Ganade de Araujo C.E., Weinberg R.F., Cordani U.G. 2013. Extruding the Borborema Province (NE-Brazil): a two-stage Neoproterozoic collision process. *Terra Nova*, **26**:157–168.
- Gill R. 2010. *Igneous rocks and processes: a practical guide*. London, Wiley-Blackwell, 428 p.
- Gioia S.M.C.L., Pimentel M.M. 2000. The Sm-Nd isotopic method in the geochronology laboratory of the University of Brasília. *Anais da Academia Brasileira de Ciências*, **72**(2):219-245. <https://doi.org/10.1590/S0001-37652000000200009>
- Gomes I.P., Rocha J.M.A., Braga I.F. 2019. Carta Geológica. *Folha SB.24-Y-B-VI – Cajazeiras*, escala 1:100.000. Estado do Ceará. Fortaleza, CPRM.
- Gorayeb P.S.S., Abreu F.A.M. 1991. O Granito do Pajé-Noroeste do Ceará: caracterização geológica. In: Simpósio de Geologia do Nordeste, 15., Recife. *Anais...*, p. 182-184.
- Gorayeb P.S.S., Abreu F.A.M., Correa J.A.M., Moura C.A.V. 1988. Relações estratigráficas entre o Granito Meruoca e a Sequência Ubajara-Jaibaras. In: Congresso Brasileiro de Geologia, 35., Belém. *Anais...*, v. 6, p. 2678-2688.
- Gorayeb P.S.S., Abreu F.A.M., Hasui Y. 1993. A tectônica distensiva e a geração de granitos eoPaleozoicos no oeste do Ceará. In: Simpósio de Geologia do Nordeste, 15., Natal. *Anais...*, p. 254-255.
- Gorayeb P.S.S., Abreu F.A.M., Santos M.V. 2014a. *Mapa geológico da Folha Frecheirinha - Ceará, escala 1:100.000*. Belém, UFPA/CPRM.
- Gorayeb P.S.S., Abreu F.A.M., Santos M.V., Silva Junior O.G. 2014b. *Mapa geológico da Folha Sobral - Ceará, escala 1:100.000*. Belém, UFPA/CPRM.
- Gorayeb P.S.S., Barbosa R.C.O., Moura C.A.V., Lemos R.L. 2011. Petrografia, geocronologia e significado tectônico do Nefelina Sienito Brejinho: extremo noroeste da Província Borborema. *Revista Brasileira de Geociências*, **41**(3):390-407.
- Gorayeb P.S.S., Coimbra C.R. 1995. O zoneamento metamórfico termal ao redor do Granito Mucambo. In: Simpósio de Geologia do Nordeste, 16., Recife. *Anais...*, v. 14, p. 337-340.
- Gorayeb P.S.S., Lafon J.M. 1995. Geocronologia Rb–Sr do Granodiorito Anil – CE. In: Simpósio de Geologia do Nordeste, 16., Recife. *Anais...*, p. 274-276.
- Gorayeb P.S.S., Lima A.M.M. 2014. Aspectos texturais do magmatismo e trama tectônica imposta ao Granito Chaval na Zona de Cisalhamento Santa Rosa, extremo noroeste da Província Borborema. *Brazilian Journal of Geology*, **44**(4):653-668. <https://doi.org/10.5327/Z23174889201400040009>
- Gorayeb P.S.S., Nascimento Y.E.S., Galarza M.A., Moura C.A.V. 2013. Novos dados geocronológicos do Granito do Pajé (Suíte Intrusiva Meruoca): magmatismo pós-tectônico no NW da Província Borborema. In: Simpósio da Província Borborema, 3., Gravatá. *Anais...*, v. 23, p. 499.
- Gorayeb P.S.S., Soares C.M. 1994. Dados petrográficos, faciologia e implicações petrológicas do Granito do Pajé. In: Congresso Brasileiro de Geologia, 38., Camboriú. *Anais...*, v. 1, p. 128-129.
- Griffin W.L., Wang X., Jackson S.E., Pearson N.J., O'Reilly S.Y., Xu X., Zhou X. 2002. Zircon chemistry and magma mixing, SE China: In situ analysis of Hf isotopes, Tonglu and Pingtam igneous complexes: *Lithos*, **61**: 237-269.
- Guimarães I.P., Silva Filho A.F., Almeida C.N., Araújo J.M.M., Sales A., Melo S.C. 1998. The Brasiliano granitoids from the Pajé-Paraíba belt and Teixeira High: Sm-Nd isotope geochemistry and U-Pb in zircon ages. In: Congresso Brasileiro de Geologia, 40., Belo Horizonte. *Anais...*, p. 48.
- Hoskin P.W.O., Black L.P. 2000. Metamorphic zircon formation by solid-state recrystallization of protolith igneous zircon. *Journal of Metamorphic Geology*, **18**(4):423-439. <https://doi.org/10.1046/j.1525-1314.2000.00266.x>
- Irvine T.N., Baragar W.R.A. 1971. A guide to the chemical classification of the common volcanic rocks. *Canadian Journal of Earth Sciences*, **8**(5):523-548. <https://doi.org/10.1139/e71-055>
- Jackson S.E., Pearson N.J., Griffin W.L., Belousova E.A. 2004. The application of laser ablation-inductively coupled plasma-mass spectrometry to in situ U–Pb zircon geochronology. *Chemical Geology*, **211**:47–69.
- Lameyre J., Bowden P. 1982. Plutonic rock types series discrimination of various granitoid series and related rocks. *Journal of Volcanology and Geothermal Research*, **14**(1-2):169-186. [https://doi.org/10.1016/0377-0273\(82\)90047-6](https://doi.org/10.1016/0377-0273(82)90047-6)
- La Roche H., Leterrier J., Grandclaude P., Marchal M.A. 1980. A classification of volcanic and plutonic rock using R1-R2 diagrams and major element analyses - its relationships and current nomenclature. *Chemical Geology*, **29**(1-4):183-210. [https://doi.org/10.1016/0009-2541\(80\)90020-0](https://doi.org/10.1016/0009-2541(80)90020-0)
- Le Maitre R.W. 2002. *A classification of igneous rocks and glossary of terms*. London, Cambridge University Press, 193 p.
- Lima A.M.M. 1997. *Caracterização petrográfica e geocronológica do Granito Chaval e das rochas encaixantes, na região de Buriti dos Lopes (PI)*. Trabalho de Conclusão de Curso de Geologia, Universidade Federal do Pará, 40 p.
- Lister G.S., Snoke 1984. S-C Mylonites. *Journal of Structural Geology*, **6**(6):617-638. [https://doi.org/10.1016/0191-8141\(84\)90001-4](https://doi.org/10.1016/0191-8141(84)90001-4)
- Ludwig K.R. 2003. *User's Manual for Isoplot/Ex version 3.00 – A Geochronology Toolkit for Microsoft Excel*, No. 4. Berkeley, Berkeley Geochronological Center, Special Publication, 70p.
- Lugmair G.W., Marti K. 1978. Lunar initial ¹⁴³Nd/¹⁴⁴Nd: Differential evolution of the lunar crust and mantle. *Earth and Planetary Science Letters*, **39**(3):349-357. [http://dx.doi.org/10.1016/0012-821X\(78\)90021-3](http://dx.doi.org/10.1016/0012-821X(78)90021-3)

- Maniar P.D., Piccoli P.M. 1989. Tectonic discrimination of granitoids. *Geological Society of America Bulletin*, **101**(5):635-643. [https://doi.org/10.1130/0016-7606\(1989\)101<0635:TDOG>2.3.CO;2](https://doi.org/10.1130/0016-7606(1989)101<0635:TDOG>2.3.CO;2)
- Mattos I.C., Artur A.C., Arthaud M.H., Nogueira Neto J.A. 2007. Geologia e geocronologia do stock granítico Serra do Barriga – Sobral/CE. In: *Simpósio de Geologia do Nordeste*, 22., Natal. *Anais...*, p. 176.
- Milhomem Neto J.M., Lafon J.M., Galarza M.A. 2017a. Lu-Hf em zircão por LA-MC-ICP-MS no Laboratório Pará-Iso (UFPA): metodologia e primeiro exemplo de aplicação na porção sudeste do Escudo das Guianas, estado do Amapá. *Contribuições à Geologia da Amazônia*, **10**:195-208.
- Milhomem Neto J.M., Lafon J.M., Galarza M.A., Moura C.A.V. 2017b. Dados Isotópicos U-Pb e Lu-Hf em Zircão para o Bloco Arqueano Amapá, Sudeste do Escudo das Guianas, Norte do Brasil. *Contribuições à Geologia da Amazônia*, **10**:333-346.
- Nascimento R.S., Gorayeb P.S.S. 2004. Basaltos da Suíte Parapuí, Gráben Jaibaras, noroeste do Ceará: caracterização, petrografia, geoquímica e química mineral. *Revista Brasileira de Geociências*, **34**(4):459-468.
- Nascimento Y.W.S. 2012. *Petrografia, litoquímica e geocronologia do Granito do Pajé: um estudo comparativo com os granitóides da Suíte Intrusiva Meruoca, região noroeste do Ceará*. Trabalho de Conclusão de Curso, Universidade Federal do Pará, Belém, 97 p.
- Nogueira B.K.C., Gorayeb P.S.S., Toro M.A.G., Moura C.A.V. 2013. Novos dados geocronológicos do Granito Chaval, extremo noroeste da Província Borborema: correlação com o Arco Magmático Santa Quitéria. In: SBG-NE, *Simpósio de Geologia do Nordeste*, 25º, Gravatá, *Anais*, CD-ROM.
- Oliveira E.C., Lafon J.M., Gioia S.M.C.L., Pimentel M.M. 2008. Datação Sm-Nd em rocha total e granada do metamorfismo granulítico da região de Tartarugal Grande, Amapá Central. *Revista Brasileira de Geociências*, **38**(1):116-129.
- Passchier C.W., Trouw R.A.J. 1998. *Microtectonics*. Berlin, Springer Verlag, 95 p.
- Paterson S.R., Vernon R.H., Zak J. 2005. Mechanical instabilities and physical accumulation of K-feldspar megacrysts in granitic magma, Tuolumne Batholith, California, USA. *Journal of the Virtual Explorer*, **18**:1-18. <https://dx.doi.org/10.3809/jvirtex.2005.00114>
- Pearce J.A., Harris N.B.W., Tindle A.G. 1984. Trace element discrimination diagrams for the tectonic interpretation of granitic rocks. *Journal of Petrology*, **25**(4):956-983. <https://doi.org/10.1093/petrology/25.4.956>
- Pitcher W.S. 1993. *The nature and origin of granite*. London: Blackie Academic and Professional. 321p.
- Rollinson H.R. 1993. *Using geochemical data: evaluation, presentation, interpretation*. New York, Longman, 352 p.
- Rubatto D. 2002. Zircon trace element geochemistry: partitioning with garnet and the link between U-Pb ages and metamorphism. *Chemical Geology*, **184**(1-2):123-138. [https://doi.org/10.1016/S0009-2541\(01\)00355-2](https://doi.org/10.1016/S0009-2541(01)00355-2)
- Russell W.A., Papanastassiou D.A., Tombrello T.A. 1978. Ca isotope fractionation on the earth and other solar system materials. *Geochimica et Cosmochimica Acta*, **42**(8):1075-1090.
- Santos T.J.S., Fetter A.H., Hackspacher P.C., Van Schmus W.R., Nogueira Neto J.A. 2008. Neoproterozoic tectonic and magmatic episodes in the NW segment of the Borborema Province, NE Brazil, during the assembly of the western Gondwana. *Journal of South American Earth Sciences*, **25**(3):271-284. <https://orcid.org/0000-0003-2125-3050>
- Santos T.J.S., Hackspacher P.C. 1992. Geologia do Grupo Martinópolis, noroeste do Ceará. In: *Congresso Brasileiro de Geologia*, 37., São Paulo. *Anais...*, v. I, p. 298-299.
- Sato K., Tassinari C.C.G. 1997. Principais eventos de acreção continental no Cráton Amazônico baseados em idade modelo Sm-Nd, calculada em evoluções de estágio único e estágio duplo. In: Costa M.L., Angélica R.S. (Eds.), *Contribuições à Geologia da Amazônia*. Belém, SBG-NO, p. 91-142.
- Shand S.J. 1950. *Eruptive rocks, their genesis, composition, classification and their relation to ore-deposits*. London, Thomas Murby, 488 p.
- Sial A.N. 1989. *Petrologia, geoquímica de elementos maiores, traços, terras raras e isótopos (Sr, O, H, S) nos batólitos de Meruoca e Mocambo, Ceará, Nordeste do Brasil*. Tese, Universidade Federal de Pernambuco, Recife, 284 p.
- Sibson R.H. 1977. Fault rocks and fault mechanisms. *Journal of Geological Society*, **133**(3):191-213. <https://doi.org/10.1144/gsjgs.133.3.0191>
- Streckeisen A.L. 1976. To each plutonic rock its proper name. *Earth Science Reviews*, **12**(1):1-33. [https://doi.org/10.1016/0012-8252\(76\)90052-0](https://doi.org/10.1016/0012-8252(76)90052-0)
- Teixeira M.F.B., Nascimento R.S., Gorayeb P.S.S., Moura C.A.V., Abreu F.A.M. 2010. Novos dados geocronológicos do Feixe de Diques de Aroeiras e sua relação com o Granito Meruoca – noroeste do Ceará. In: *Congresso Brasileiro de Geologia*, 45., Belém. *Anais...* CD-ROM.
- Thompson R.N. 1982. Magmatism of the British Tertiary volcanic province. *Scottish Journal of Geology*, **18**:49-107. <https://doi.org/10.1144/sjg18010049>
- Trouw R.A.J., Passchier C.W., Wiersma D.J. 2010. *Atlas of mylonites and related microstructures*. Berlin, Springer-Verlag, 322 p.
- Vernon R.H. 2008. *A practical guide to rock microstructures*. Cambridge, Cambridge University Press, 594 p.
- Whalen J.B., Currie K.I., Chappell B.W. 1987. A-type granites: geochemical characteristics, discrimination and petrogenesis. *Contribution to Mineralogy and Petrology*, **95**:407-419. <https://doi.org/10.1007/BF00402202>
- White S.H., Burrouws S.E., Carreras J., Shaw N.D., Humphreys F.J. 1980. On mylonites in ductile shear zones. *Journal of Structural Geology*, **2**(1-2):175-187. [https://doi.org/10.1016/0191-8141\(80\)90048-6](https://doi.org/10.1016/0191-8141(80)90048-6)
- Wilson M. 1989. *Igneous Petrogenesis: a global tectonic approach*. London, Unwin Hyman, 466 p.